



## Temperature Dependence of the Electroclinic Effect in the Twist-Bend Nematic Phase

Claire Meyer, Patrick Davidson, Geoffrey Luckhurst, Irena Dokli, Anamarija Knežević, Andreja Lesac, Daniel Paterson, Rebecca Walker, John Storey, Corrie Imrie, et al.

### ► To cite this version:

Claire Meyer, Patrick Davidson, Geoffrey Luckhurst, Irena Dokli, Anamarija Knežević, et al.. Temperature Dependence of the Electroclinic Effect in the Twist-Bend Nematic Phase. *Crystals*, 2023, 13 (3), pp.465. 10.3390/cryst13030465 . hal-04067242

**HAL Id: hal-04067242**

**<https://u-picardie.hal.science/hal-04067242>**

Submitted on 20 Nov 2023

**HAL** is a multi-disciplinary open access archive for the deposit and dissemination of scientific research documents, whether they are published or not. The documents may come from teaching and research institutions in France or abroad, or from public or private research centers.

L'archive ouverte pluridisciplinaire **HAL**, est destinée au dépôt et à la diffusion de documents scientifiques de niveau recherche, publiés ou non, émanant des établissements d'enseignement et de recherche français ou étrangers, des laboratoires publics ou privés.

# Article

## Temperature Dependence of the Electroclinic Effect in the Twist-Bend Nematic Phase

Claire Meyer <sup>1</sup>, Patrick Davidson <sup>2</sup>, Geoffrey R. Luckhurst <sup>3</sup>, Irena Dokli <sup>4</sup>, Anamarija Knežević <sup>4</sup>, Andreja Lesac <sup>4</sup>, Daniel A. Paterson <sup>5</sup>, Rebecca Walker <sup>5</sup>, John M.D. Storey <sup>5</sup>, Corrie T. Imrie <sup>5</sup>, and Ivan Dozov <sup>\*1,2</sup>

<sup>1</sup> PSC, Université de Picardie Jules Verne, 80039 Amiens, France

<sup>2</sup> Laboratoire de Physique des Solides, Université, Paris-Saclay, CNRS, 91405 Orsay, France

<sup>3</sup> School of Chemistry, Faculty of Engineering and Physical Sciences, University of Southampton, Southampton SO17 1BJ, United Kingdom

<sup>4</sup> Rudjer Boskovic Institute, Bijenicka 54, 10000 Zagreb, Croatia

<sup>5</sup> Department of Chemistry, School of Natural and Computing Sciences, University of Aberdeen, Meston Building, Aberdeen AB24 3UE, UK

\* Corresponding author: [ivan.dozov@u-psud.fr](mailto:ivan.dozov@u-psud.fr)

**Abstract:** The twist-bend nematic ( $N_{TB}$ ) phase of bent-shaped molecules has recently attracted much attention due to the spontaneous bend of its director field and the doubly-degenerate chirality of its heliconical structure. Despite intensive experimental and theoretical investigation worldwide, the main structural characteristics (pitch and conical angle) and elastic properties of the phase are still barely understood. This is mainly due to the difficulty in growing large single domains of the  $N_{TB}$  phase, which prevents the application of the powerful electro-optical techniques developed for the nematic (N) phase. Moreover, the twist and bend distortions of the optic axis are forbidden by the pseudo-layered structure of the  $N_{TB}$  phase, which makes its response to the field smectic-like instead of nematic-like. Therefore, the only macroscopic electric effect that can be observed deep in the  $N_{TB}$  phase is the smectic-like “electroclinic” effect ( $EC_{ENTB}$ ). Here, we achieve large monochiral  $N_{TB}$  domains which remain uniform over a wide temperature range (20 – 60 °C) in thin (1.5  $\mu\text{m}$ ) planar cells, thus avoiding the so-called stripe- and rope-like textural instabilities. This allowed us to experimentally determine using electro-optical measurements the temperature dependence of the  $EC_{ENTB}$  response in four different  $N_{TB}$  materials: namely the dimers CB7CB, CB9CB, CB6OCB, and BNA76. For all compounds, the thermal dependences of conical angle and pitch in the vicinity of the N- $N_{TB}$  transition follow the theoretically predicted power-law behaviour. However, the agreement between the measured and predicted power-law exponents remains only qualitative, which calls for improvement of the theoretical models.

**Keywords:** liquid crystal; twist-bend nematic; electro-clinic effect

**Citation:** *Crystals* 2022, 12, x. <https://doi.org/10.3390/xxxxx>

Academic Editor:

Received:

Accepted:

Published: date

**Publisher’s Note:** MDPI stays neutral with regard to jurisdictional claims in published maps and institutional affiliations.



**Copyright:** © 2022 by the authors. Submitted for possible open access publication under the terms and conditions of the Creative Commons Attribution (CC BY) license (<https://creativecommons.org/licenses/by/4.0/>).

### 1. Introduction

The most common liquid-crystalline phase, the nematic phase, is characterized by the orientational order of its anisotropic molecules and the absence of positional order. When the molecules are rod-like and achiral, they form the conventional nematic phase (N) in which the molecules orient with their long axes approximately oriented parallel to a common direction called the nematic director,  $\mathbf{n}$ . In the ground state, the director is uniform but, under external constraints, it can be distorted, which gives rise to an elastic distortion energy [1]:

$$f^n = \frac{1}{2} \left\{ K_{11} [\mathbf{n}(\nabla \cdot \mathbf{n})]^2 + K_{22} [\mathbf{n} \cdot (\nabla \times \mathbf{n})]^2 + K_{33} [\mathbf{n} \times (\nabla \times \mathbf{n})]^2 \right\}, \quad (1)$$

where  $K_{11}$ ,  $K_{22}$ , and  $K_{33}$  are the elastic moduli for the three eigenmodes of the director distortion: splay  $\mathbf{n}(\nabla \cdot \mathbf{n})$ , twist  $\mathbf{n} \cdot (\nabla \times \mathbf{n})$ , and bend  $\mathbf{n} \times (\nabla \times \mathbf{n})$ , respectively.

When the molecules are chiral, they form chiral modifications of the nematic phase. In the most common one, the chiral nematic (or cholesteric),  $N^*$ , the director is spontaneously twisted and the molecules are arranged on a right-angle helix with axis  $\mathbf{h}$ , such that  $\mathbf{h} \perp \mathbf{n}$ .

Yet other nematic phases are expected for molecules with shape different from rod-like, e.g. biaxial molecules were predicted [2] to form a thermotropic biaxial nematic phase,  $N_b$ . Another long-standing theoretical prediction [3-6] was that bent-shaped molecules can form nematic phases with a spontaneously bent director, namely the splay-bend nematic,  $N_{SB}$ , and twist-bend nematic,  $N_{TB}$ , phases. Two distinct origins of the spontaneous bend have been proposed: either the coupling of a flexoelectric polarization with a transverse ferroelectric polarization of the nematic [3,4] or an elastic instability of the phase due to the natural tendency of the bent-shaped molecules to orient parallel to a curved director [5,6]. For a long time, neither of these arguments attracted much attention, until the  $N_{TB}$  phase was experimentally identified in the bent-shaped mesogenic dimer CB7CB [7]. As predicted, the molecules in the  $N_{TB}$  phase form a conical helix, with helix axis  $\mathbf{h}$ , pitch  $p$ , and long molecular axis  $L$  parallel to the local director  $\mathbf{n}$ , that is tilted at an angle  $\theta$  with respect to  $\mathbf{h}$  (see Figure 1). Moreover, the structure is locally biaxial, the curvature of the bent-shaped molecule matching the curvature of the director field and thus, the bend vector,  $\mathbf{b} = \mathbf{n} \times (\nabla \times \mathbf{n})$  ( $\mathbf{b} \perp \mathbf{n}$ ), is a secondary director of the nematic order tensor. Due to its heliconical structure, the  $N_{TB}$  phase is chiral, even when it is formed by achiral molecules. The chiral symmetry of the phase is spontaneously broken [5] and two different structures are possible, with left or right handedness of the conical helix. These chiral structures can coexist in the sample forming large monochiral domains suitable for optical and electro-optical observations [8-10].

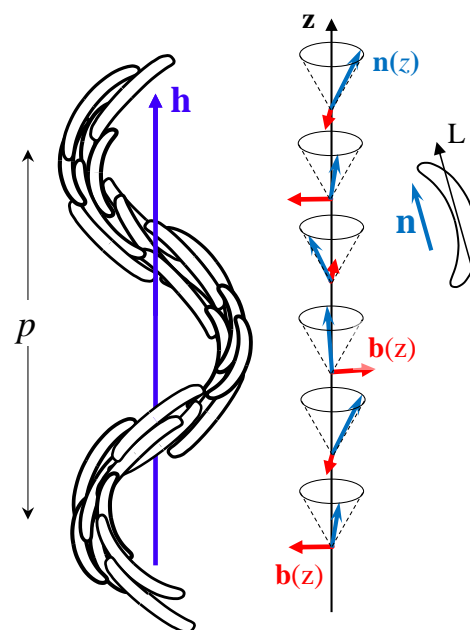


**Figure 1.** Heliconical structure of the  $N_{TB}$  phase. The long axes,  $L$ , of the bent-shaped molecules are on average oriented parallel to the nematic director,  $\mathbf{n}$ . Along the helix axis,  $\mathbf{h}$ , the director rotates

and follows a conical helix with pitch  $p$ . The bend vector,  $b$ , is organized on a right-angle helix. (The helical structure is doubly degenerate but only the right handedness is shown here for simplicity.).

The discovery of the  $N_{TB}$  phase generated great interest and stimulated further chemical and physical studies. Hundreds of new bent-shaped mesogenic dimers presenting this phase have been synthesized (see [11,12] for recent reviews) and the  $N_{TB}$  helical structure was confirmed [7,9,13–20] using a large number of techniques. X-ray scattering studies confirmed that the phase is indeed nematic, with no long-range positional order [7,14,21–24]. The early indirect prediction [9,25] of the extremely small pitch of the helix,  $p < 10$  nm, was then quickly confirmed by direct freeze-fracture transmission electron microscopy studies [13,14] and later by resonant X-ray scattering experiments [18,19,26]. The values of  $p$  reported for different  $N_{TB}$ -forming compounds are always of the order of 10 nm and slowly decrease with decreasing temperature.

The second important structural parameter of the phase, the conical tilt angle  $\theta$ , has also been measured for a few compounds [10,13,17,27]. It is small at the  $N$ - $N_{TB}$  transition,  $\theta < 10^\circ$  for CB7CB, and even close to zero when the phase transition is very weakly first order. As theoretically expected,  $\theta$  increases up to  $30$ – $40^\circ$  far below the transition temperature.

Despite its lack of long-range positional order, due to its layered structure, the  $N_{TB}$  phase behaves in several aspects as a smectic (Sm) phase. It shows typical smectic textures, such as focal-conics, fan-shaped textures, and stripe- and rope-textures [7], both in sandwich cells and as free drops. In biphasic coexistence with the conventional nematic phase, the  $N_{TB}$  phase forms structures almost identical to the “bâtonnets” observed during the growth of the smectic A (SmA) phase from an isotropic melt [28]. The macroscopic elastic properties of the  $N_{TB}$  phase and its response to external fields are also smectic-like [7,9,29–31]. This prevents applying to it the efficient and accurate electric and electro-optical techniques developed for the conventional nematic phase, thus limiting the choice of tools available to investigate its physical properties.

This smectic-like behaviour has been shown to result from the pseudo-layered structure of the  $N_{TB}$  phase [29,31]. The periodic mass-density wave of the smectic phase, which gives rise to the smectic layers, is absent in the  $N_{TB}$  phase, but instead a periodic distortion wave takes place because the planes perpendicular to the helix axis, which correspond to the same azimuthal orientation of the director, form a set of equidistant “pseudo-layers”. This pseudo-layered structure, which is quite similar to the well-known pseudo-layered structure of the cholesteric phase [29], is responsible for the smectic-like elastic properties at large length scale ( $\gg p$ ).

Macroscopically, a monochiral domain of the  $N_{TB}$  phase is periodic in one dimension (due to the pseudo-layering), uniaxial (due to the  $D_\infty$  global symmetry of the helix axis), and chiral (due to the helix handedness). This symmetry is in fact the same as that of the chiral smectic A (SmA\*) phase, which allowed for the coarse-grained (CG) description of the  $N$ - $N_{TB}$  phase transition [31,32], by analogy with the de Gennes theory [33] of the  $N$ -SmA phase transition. This CG approach provides the description of all the macroscopic properties of the twist-bend nematic [31,32]: for example, the smectic-like elasticity, response to external fields, and surface anchoring. Moreover, after choosing one of the available microscopic models [5,34] of the  $N$ - $N_{TB}$  phase transition, the CG model allows one to calculate all the macroscopically relevant parameters and their temperature dependences in the  $N_{TB}$  phase from the microscopic properties of the  $N$ -phase.

Based on the  $N_{TB}$ -SmA\* analogy, some of the electro-optic effects of the SmA\*, such as the electroclinic effect (ECE) [35], can be expected to have  $N_{TB}$  analogs, such as the  $ECE_{N_{TB}}$  in the  $N_{TB}$  phase [9]. Although the physical origin differs in the two cases (ferroelectricity in SmA\* instead of flexoelectricity in  $N_{TB}$ ), the result is the same: under a strong field, the distortion of the periodic structure results in a fast rotation of the optical

axis with respect to the normal to the (pseudo)layers. Despite the small amplitude of the effect, it can be measured precisely over a large temperature range [9] in the  $N_{TB}$  phase, giving valuable (although semi-quantitative) information about the phase structure. However, due to some experimental issues (mainly the difficulty to obtain large monochiral domains and to keep them uniform, deep in the  $N_{TB}$  phase), a precise study of the  $EC_{ENTB}$  has only been reported so far for CB7CB, even though it was qualitatively described for a few other compounds [22,36,37].

Here, we study experimentally the temperature dependence of the  $EC_{ENTB}$  response in four different  $N_{TB}$  materials, the dimers CB7CB [7,20,38], CB9CB [15], CB6OCB [16], and BNA76 [39]. In thin planar cells, we achieve large monochiral domains which remain uniform over a wide temperature range. We measure the temperature dependences of the amplitude and the characteristic time of the  $EC_{ENTB}$  response in all four compounds and compare with their theoretically predicted behaviours. The agreement of the experimental results with the theory remains only qualitative, suggesting the need to further improve the theoretical models.

## 2. Theoretical background

In this section, we recall a few key points of the theory of the  $EC_{ENTB}$  and its coarse-grained description that have been reported in detail elsewhere [5,31,34,37,40].

### 2.1. $N_{TB}$ -SmA\* analogy and CG description of the $N_{TB}$ phase

On a large scale, due to its periodicity, the structure of the  $N_{TB}$  phase is similar to that of the SmA\*. The unperturbed SmA\* state is uniaxial, with  $D_\infty$  symmetry axis along the director  $\mathbf{n}_0$ , which is also the optic axis of the phase, and the mass density  $\rho$  is modulated along  $\mathbf{n}_0$ , with wave vector  $\mathbf{q}_0 = q_0 \mathbf{n}_0$ , where  $q_0 = 2\pi/d$  and  $d$  is the layer thickness (see Fig. 2a). When the SmA\* phase is distorted, the director  $\mathbf{n}(\mathbf{r})$  and the positions of the layers vary slowly in space, and this distortion costs some elastic energy. To describe the structure of the SmA phase and its elastic properties, de Gennes [33] introduced a complex order parameter  $\psi = |\psi| \exp(i\phi)$ , where  $|\psi|$  is the amplitude of the mass-density wave and  $\phi$  is the phase which describes the local layer displacement,  $u = d\phi/2\pi$ , and varies slowly in space.

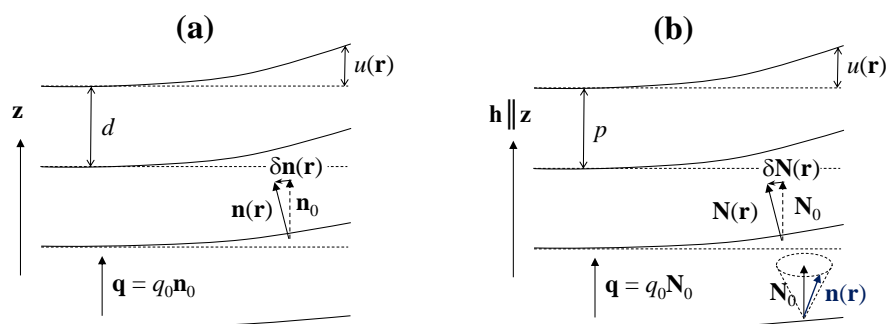


**Figure 2.** Analogy between the layered structure of the SmA\* phase (a) and the pseudo-layered structure of the  $N_{TB}$  phase (b).

The distortion wave of the local director  $\mathbf{n}$  along the helix axis  $\mathbf{h}$  in the  $N_{TB}$  phase is analogous to the density wave in the smectic. Accordingly, the  $N_{TB}$  phase can be considered as a stack of pseudo-layers, perpendicular to  $\mathbf{h}$ , with a very small period,  $p \sim 10$  nm. At a much larger, macroscopic, scale, the phase is uniaxial with symmetry axis defined by

the optic axis  $\mathbf{N}$  – a unit vector pointing along the average orientation of the director  $\mathbf{n}$  over one helical period, i.e., along the axis of the helical cone (see Fig. 2b). By analogy with the SmA\* phase, the structure of the N<sub>TB</sub> and its elastic properties can be described by a complex order parameter,  $\sigma(\mathbf{r}) = \sin \theta(\mathbf{r}) \exp(i\varphi(\mathbf{r}))$  [31]. When  $\theta(\mathbf{r})$  and  $\mathbf{q}(\mathbf{r}) = \nabla \varphi(\mathbf{r})$  are close to their equilibrium values and vary slowly with  $\mathbf{r}$ , the macroscopic elastic energy of the N<sub>TB</sub> is formally the same [31] as that of the SmA\* [33]. It contains smectic-like terms, e.g., the pseudo-layer compression term,  $\frac{1}{2} B (1 - p/p_0)^2$ , taking account of the increase in the energy density when the pitch,  $p$ , deviates from its equilibrium value,  $p_0$ . Another important smectic-like term,  $\frac{1}{2} K_{\delta N} \sin^2 \alpha$ , takes into account the energy cost for the tilt of the optic axis  $\mathbf{N}$  by a small angle  $\alpha$  with respect to the helix axis,  $\mathbf{h}$  ( $\mathbf{N}$  is parallel to  $\mathbf{h}$  in the ground state but can deviate from  $\mathbf{h}$  under external constraints). Additionally, the energy contains three nematic-like terms,

$$f^N = \frac{1}{2} \left\{ K_{11}^N [\mathbf{N}(\nabla \cdot \mathbf{N})]^2 + K_{22}^N [\mathbf{N} \cdot (\nabla \times \mathbf{N})]^2 + K_{33}^N [\mathbf{N} \times (\nabla \times \mathbf{N})]^2 \right\}, \quad (2)$$

which are related to the splay, twist, and bend of the optic axis, where  $K_{ii}^N$  are the respective elastic moduli. As in the SmA phase, the twist and the bend of  $\mathbf{N}$  are forbidden because they are incompatible with the pseudo-layered structure of the phase. Moreover, the splay distortion of  $\mathbf{N}$  is coupled with a splay of the helix axis, which requires a reorganization of the layers and is strongly hindered in confined samples.

The N<sub>TB</sub> – SmA\* analogy provides the general expression for the macroscopic elastic energy of the distorted N<sub>TB</sub> phase but not the values of the elastic moduli. However, these moduli can be obtained by coarse-graining a microscopic model of the N – N<sub>TB</sub> phase transition [5,34]. For this purpose, one should consider a large-wavelength distortion of the phase having a small amplitude. The energy cost of the distortion is calculated using the microscopic model and the result is averaged over one pitch length, thus removing all of the periodic terms. The comparison of this microscopic result with the macroscopic elastic energy then provides the values of the elastic moduli.

This CG approach has been applied in [31], starting from the “elastic instability” model of the N – N<sub>TB</sub> phase transition [5]. The basic assumption of this model is that the elastic constant  $K_{33}$  of the nematic formed by bent-shaped molecules decreases with decreasing temperature  $T$  and becomes negative at some  $T = T^*$ . Therefore, for  $T < T^*$ , the ground state of the nematic is no longer uniform but it is spontaneously bent. However, as explained earlier, the bend distortion must be coupled to another distortion mode which is the twist mode in the case of the N<sub>TB</sub> phase. Introducing a fourth-order bend elastic modulus,  $C > 0$ , and assuming that  $K_{33}$  varies linearly with temperature in the vicinity of  $T^*$ ,  $K_{33} = a(T - T^*)$ , with  $a > 0$ , and that all of the other nematic moduli remain approximately constant, one obtains [5], after minimization of the energy, that the ground-state structure of the phase is helical, with  $\mathbf{n}(z) = (\sin \theta_0 \cos q_0 z, \sin \theta_0 \sin q_0 z, \cos \theta_0)$ , where  $\mathbf{z} \parallel \mathbf{h}$ . Under these assumptions, the system undergoes a second-order phase transition at  $T = T^*$  and, close to  $T^*$ , the equilibrium tilt angle and wave vector of the helix are given by:

$$\sin^2 \theta_0 = -\frac{K_{33}}{3K_{22}} = -\frac{a}{3K_{22}}(T^* - T) \quad ; \quad q_0^2 = -\frac{K_{33}}{3C} = \frac{a}{3C}(T^* - T) \quad . \quad (3)$$

Therefore,  $\sin \theta_0(T)$  and  $q_0(T)$  are expected to follow power laws,  $Const \cdot (T^* - T)^\beta$  with the same critical exponent,  $\beta_\theta = \beta_q = 1/2$ .

An alternative microscopic model for the N-N<sub>TB</sub> phase transition was proposed by Shamid et al. [34]. In that model, the transition is driven by the strong flexoelectric polarization expected in a nematic formed by bent-shaped molecules. Due to the strong flexoelectric fluctuations in the pretransitional nematic range, the effective bend modulus,  $K_{33}^{eff}$ , renormalized by the flexoelectric effect, decreases with decreasing temperature, and changes sign at the N-N<sub>TB</sub> transition. Therefore, despite the different physical origins of the transition, that model also predicts a second-order phase transition at  $T = T^*$  and, close to  $T^*$ , the behaviour of the tilt angle and wave vector follow power laws:

$$\sin^2 \theta_0 = C_\theta (T^* - T) \quad ; \quad q_0^2 = C_q (T^* - T) \quad , \quad (4)$$

where  $C_\theta$  and  $C_q$  are functions of the nematic constants, whose temperature dependence can be neglected close to the N-N<sub>TB</sub> transition.

A more refined version of the same theoretical model has been used to build a CG theory of the N<sub>TB</sub> phase [40]. It again predicts a second-order N-N<sub>TB</sub> transition at some temperature  $T^*$ , but with a more complex temperature dependence of  $\theta_0$  and  $q_0$ . This dependence shows a crossover of the power-law exponents for  $\theta_0$  and  $q_0$  at some temperature  $T^* - \delta T$ , where  $\delta T$  was found to be very small for the N<sub>TB</sub>-forming mixture studied in [40]. Indeed, for  $T^* > T > T^* - \delta T$ , the exponents are the same as in Eq. (4),  $\beta_\theta = \beta_q = 1/2$ , while for  $T < T^* - \delta T$  they become  $\beta_\theta = \beta_q = 1/4$ .

## 2.2. Behaviour under external fields

The response of the N<sub>TB</sub> phase to strong external fields, e.g., when an electric field,  $E$ , is applied, is expected to be different on the microscopic ( $< p$ ) and macroscopic ( $>> p$ ) scale. Microscopically, the response is nematic-like, with a local director,  $\mathbf{n}$ , reorientation inside the heliconical period, resulting in variation of the pitch and tilt angle [9,30,41], distortion of the helix from circular to elliptic [9,30], or field-induced transition to the nematic [30,41] or splay-bend nematic [42] phases. Due to the small pitch, the N<sub>TB</sub> phase is expected to be very stiff and these effects very small for realistically strong fields. Indeed, no experimental evidence has been provided so far for this microscopic effect of the field, except for the N<sub>TB</sub> to N<sub>SB</sub> transition under a strong topological constraint [10] or strong electric field [42],  $E \sim 8 \text{ V}/\mu\text{m}$ .

In addition to this local response of  $\mathbf{n}$ , the torque integrated over a large volume of the N<sub>TB</sub> phase acts on the optic axis  $\mathbf{N}$  and can drive its reorientation. This macroscopic response may (or may not) be coupled with a reorientation of the helix axis. Indeed, the pseudo-layered structure of the phase forbids the bend and twist of  $\mathbf{N}$  in a defect-free N<sub>TB</sub> domain. The splay of  $\mathbf{N}$  under a field, although not forbidden, is also hindered in most sample geometries because it requires the reorientation and displacement of the pseudo-layers (large splay distortion leads also to layer dilation, which is energetically prohibitively costly). Consequently, smooth, continuous, and defect-less textural changes similar to the Fréedericksz transition in nematics are impossible in the N<sub>TB</sub> phase. Instead, in sufficiently strong fields, a large macroscopic N<sub>TB</sub> domain can reorient by coupled rotation of  $\mathbf{N}$  and  $\mathbf{h}$ , giving rise to the nucleation of many defects, located either in the bulk or at the grain-boundaries separating the reoriented domain from the adjacent regions. This kind of irreversible, defect-mediated, effect was reported experimentally under moderate electric fields [7,43].

Because it has the same macroscopic symmetry as that of the SmA\* phase, the twist-bend nematic phase should present some specific SmA\*-like effects, for example the electroclinic effect (ECE) [35]: under an electric field  $\mathbf{E}$ , applied parallel to the SmA\* layers, the director  $\mathbf{n}$  tilts at an angle  $\alpha$  with respect to the normal  $\mathbf{k}$  to the layers, in a plane

perpendicular to  $\mathbf{E}$  (see Fig. 3a). This effect can be understood as a field-induced SmA\* - SmC\* phase transition: in the SmC\*, under field, the director  $\mathbf{n}$  is tilted with respect to  $\mathbf{k}$  and the phase is ferroelectric, with the polarization  $\mathbf{P}_{fer}$  proportional to  $\mathbf{n} \times \mathbf{k}$ . In the SmA\*, due to  $\mathbf{n} \parallel \mathbf{k}$ ,  $\mathbf{P}_{fer}$  vanishes, but when the field is applied, it induces a director tilt and a ferroelectric polarization,  $\mathbf{P}_{fer} \neq \mathbf{0}$ , with resulting energy gain  $-\mathbf{E} \cdot \mathbf{P}_{fer}$  (i.e. ECE is an inverse ferroelectric effect). The smectic elasticity, however, disfavors the tilt, and the energy minimization gives  $\sin \alpha = c_\alpha E$ , where  $c_\alpha$  is the electroclinic coefficient. Typically, due to the stiff SmA elasticity,  $\alpha$  is very small ( $\alpha \ll 1^\circ$ ) even in strong fields, but much higher amplitudes have been reported in the vicinity of a SmA\* - SmC\* phase transition. For symmetry reasons, the smectic C ferroelectricity and the ECE are forbidden in an achiral medium. Indeed, the polarization  $\mathbf{P}_{fer}$  is a true vector, while  $\mathbf{n} \times \mathbf{k}$  is a pseudo-vector, so that their proportionality coefficient should be a pseudo-scalar, which cannot exist in an achiral system. Moreover, because the ECE response is linear in the field, the sign of  $\alpha$  should change with the sign of  $E$ , as well as with the chirality handedness.

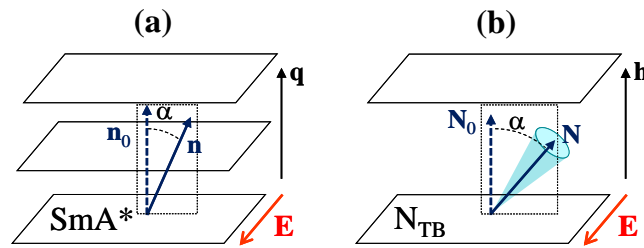


**Figure 3.** Electroclinic effect in the SmA\* (a) and  $N_{TB}$  (b) phases. When the field is applied in the plane of the SmA\* layers, the director  $\mathbf{n}$  rotates in a plane perpendicular to  $\mathbf{E}$  and tilts at an angle  $\alpha$  with respect to the normal to the layers. Similarly, when an electric field is applied in a direction parallel to the  $N_{TB}$  pseudo-layers, the optic axis,  $\mathbf{N}$ , tilts away at an angle  $\alpha$  from the helix axis,  $\mathbf{h}$ , in a plane perpendicular to  $\mathbf{E}$ . In fact, the whole director cone (the shaded region) tilts by the same angle  $\alpha$ , without much distortion..

Just after the discovery of the  $N_{TB}$  phase, a fast linear electro-optic effect was observed in it [36] and has been reported as an analogue of the flexo-electric effect seen for cholesterics [44]. A detailed theoretical analysis [9] later showed that this effect is the  $N_{TB}$  counterpart,  $ECE_{NTB}$ , of the ECE in the SmA\* phase. As in the SmA\*, when a d.c. electric field  $\mathbf{E}$  is applied parallel to the pseudo-layers of a  $N_{TB}$  monochiral domain (see Fig. 3b), the optic axis  $\mathbf{N}$  tilts away from the helix axis  $\mathbf{h}$  at an angle  $\alpha$  proportional to the field amplitude. Although  $ECE_{NTB}$  and ECE have the same geometry, their physical origins differ in that the former is due to the flexoelectricity whereas the latter is due to the ferroelectricity. Indeed, as in usual nematics, the director distortion in the  $N_{TB}$  phase results in a flexoelectric polarization,  $\mathbf{P}_{fl} = e_1 \mathbf{n} (\nabla \cdot \mathbf{n}) - e_3 \mathbf{n} \times (\nabla \times \mathbf{n})$ , where  $e_1$  and  $e_3$  are Meyer's splay and bend flexoelectric coefficients [45]. In the ground state of the  $N_{TB}$  phase, the splay is negligible but the bend is strong, giving rise to a large polarization perpendicular to both  $\mathbf{h}$  and  $\mathbf{n}$ , and forming an orthogonal helix. Due to this heli-electric organization, the total flexo-polarization of the phase averages to zero. However, it has been shown that a uniform tilt of the optic axis leads to excess average flexoelectric polarization,  $\langle \mathbf{P}_{fl} \rangle \propto \mathbf{N} \times \mathbf{h}$ , which results, under an applied field  $\mathbf{E}$ , in an energy density gain  $\langle f_{fl} \rangle = -\langle \mathbf{P}_{fl} \rangle \cdot \mathbf{E}$ . The straightforward CG calculation and minimization of the energy gives the amplitude of the  $ECE_{NTB}$  tilt angle [9]:



$$\alpha \approx \tan \alpha = c_{\alpha} E = \frac{e_1 - e_3}{q_0 (K_{11} + K_{22})} E, \quad (5)$$

where  $q_0 = \pm 2\pi / p$  is the equilibrium value of the  $N_{TB}$  wavenumber (with its sign depending on the handedness of the domain). The values and the temperature dependences of the constants  $e_1 - e_3$ ,  $K_{11}$ , and  $K_{22}$  in the  $N_{TB}$  phase are unknown, but as a reasonable approximation it may be assumed that they are continuous at the  $N-N_{TB}$  transition and that their thermal variation is negligible compared to the fast variation of  $K_{33}$  and  $q_0$ . Therefore, the electroclinic coefficient  $c_{\alpha}$  is expected theoretically to vary as  $c_{\alpha} : (T^* - T)^{-\beta_{\alpha}}$ , where the critical exponent is either  $\beta_{\alpha} = 1/2$  [9,31] or shows a cross-over from  $1/2$  to  $1/4$  at  $T = T^* - \delta T$  [40].

The CG approach also gives a simple result for the time dependence of the ECE tilt angle,  $\alpha(t)$ , when the field is switched on or off [9]. In the off-case,  $\alpha(t)$  follows an exponential law,  $\alpha_{off}(t) = \alpha_0 \exp(-t / \tau_{off})$ , with initial value  $\alpha_0$  given by Eq. (5). Similarly, in the on-case, the dependence is given by  $\alpha_{on}(t) = \alpha_0 [1 - \exp(-t / \tau_{on})]$  and the two characteristic times are in fact the same [9]:

$$\tau = \tau_{off} = \tau_{on} = \frac{2\gamma_1}{(K_{11} + K_{22}) q_0^2 \sin^2 \theta_0} \quad (6)$$

where  $\gamma_1$  is the rotational viscosity of the nematic, which is expected to be continuous at the  $N-N_{TB}$  transition and to follow an Arrhenius law on cooling. In the vicinity of the transition, for both microscopic models of the  $N-N_{TB}$  transition, a power-law behaviour of the response time is expected,  $\tau : (T^* - T)^{-\beta_{\tau}}$ , where the critical exponent is either  $\beta_{\tau} = 2$  [9,31] or shows a cross-over from 2 to 1 at  $T = T^* - \delta T$  [40].

To date, precise  $ECE_{NTB}$  measurements have been reported only for CB7CB, showing a very fast effect ( $\tau < 1 \mu s$ ), with a small amplitude ( $\alpha < 1^\circ$  for  $E = 10 \text{ V}/\mu m$ ) [9]. Qualitatively, these results confirmed several important features predicted by Eqs. (5-6): the tilt angle increases linearly with  $E$  and changes sign with that of the field and with the handedness of the studied monochiral domain; the time-dependence of the tilt angle is exponential and shows the same response time for both the rise and fall. Estimating the values of  $e_1 - e_3$ ,  $K_{11}$ ,  $K_{22}$ , and  $\gamma_1$  from their usual nematic values, it was inferred that, close to the  $N-N_{TB}$  transition, the pitch is extremely small,  $p \approx 7 \text{ nm}$  [9,25], a value that was later confirmed by more direct techniques [13,14,19].

The electroclinic effect in the  $N_{TB}$  phase is interesting for two main reasons. On one side, its fast, sub-microsecond, response times are very attractive for practical applications, despite the disappointingly small tilt angle. Therefore, it is important to study a larger number of compounds showing the  $N_{TB}$  phase to check whether these values are typical and whether they can be optimized. From a more fundamental point of view, the ECE technique is one of the few that can be applied, without hysteresis and reversibility issues, to test some basic structural parameters of the  $N_{TB}$  phase over a large temperature range, thus providing an opportunity to discriminate between the available theoretical models. Moreover, we demonstrate here that the experimental difficulties (related to the small values of  $\alpha$  and  $\tau$ , and especially, to the realization of the required large, uniform, monochiral domains) that have so far hampered the investigation of the ECE, can be easily overcome to gather useful information about the  $N_{TB}$  phase.

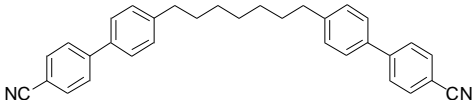
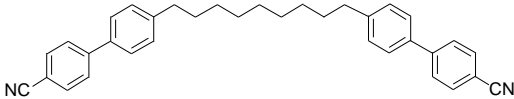
### 3. Materials and methods

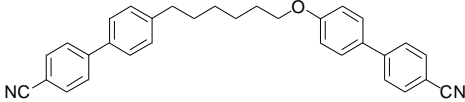
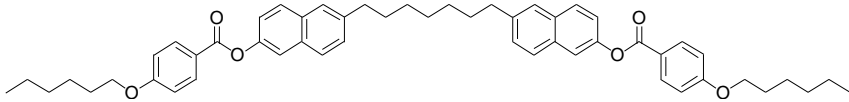
#### 3.1. $N_{TB}$ -forming mesogenic dimers

We studied four different compounds, showing both the N and  $N_{TB}$  phases, that were chosen according to three criteria: i) a wide temperature range of the  $N_{TB}$  phase to avoid crystallization of the samples during the experiments; ii) the ability to obtain uniform monochiral domains sufficiently large for the ECE measurements; iii) selection of different dielectric anisotropy (positive or negative) and different strength of the weakly first order N- $N_{TB}$  phase transition (to test the influence of these parameters on the ECE amplitude and the temperature dependences of  $\alpha$  and  $\tau$ ).

The chemical structures of the compounds are presented in Table 1. All of them are mesogenic dimers of two identical monomers connected by an alkyl or alkoxy spacer consisting of odd-number groups. For all of them, in an all-trans conformation of the spacer, the dimer is strongly bent. Due to the flexibility of the spacer, a large number of conformers are possible, but most of them are also bent. Therefore, on average, the dimer molecule is typically bent by a 120–130° angle between the monomers. This strongly bent shape of the mesogenic molecule has been predicted [5,6] and experimentally confirmed [7,15] to be an essential condition for the formation of the  $N_{TB}$  phase. Table 1 also presents the phase transition temperatures observed in our electro-optical experiments upon cooling for each compound. Note that they differ in some cases by as much as 2°C from those measured by DSC. This difference is mainly due to two factors: i) the very different cooling rates in the two cases ( $\geq 5$  °C/min for DSC and  $\leq 0.1$  °C/min in our experiments); ii) the different surface/volume ratios in the two experiments. This ratio is much larger in our thin sandwich cells, leading to some diffusion in the sample of impurities from the alignment layers and sealing walls of the cell (this contamination leads to a shift in the transition temperatures but does not significantly influence our ECE experiments).

**Table 1.** Molecular structure and phase transition temperatures of the mesogenic dimers. The temperatures are measured on cooling in our thin sandwich cells. The biphasic coexistence range and its median temperature,  $T_c$ , are shown for the N- $N_{TB}$  phase transition. Also shown, in brackets, are the melting points of the crystal/solid which gives the  $N_{TB}$  phase for the three cyanobiphenyl dimers [15] and that containing two naphthalene groups [39]. These are included to show that thermodynamically the twist-bend nematic range can be extremely short; however this range can be significantly extended as early studies, especially for CB7CB, have shown [7].

Compound	Molecular Structure and Phase Transition Temperatures
CB7CB	 <p>Iso - 114.8 °C - N - 99.85 ± 0.35 °C - <math>N_{TB}</math> - 37 °C - Cr (Cr - 102 °C - <math>N_{TB}</math>)</p>
CB9CB	 <p>Iso - 124.1 °C - N - 107.00 ± 0.0 °C - <math>N_{TB}</math> - 41 °C - Cr (Cr - 86 °C - <math>N_{TB}</math>)</p>

<b>CB6OCB</b>	 <p><b>Iso</b> - 156.6 °C - <b>N</b> - 108.08 ± 0.03 °C - <b>N<sub>TB</sub></b> - 80 °C - <b>Cr</b>      (<b>Cr</b> - 99 °C - <b>N<sub>TB</sub></b>)</p>
<b>BNA76</b>	 <p><b>Iso</b> - 153.1 °C - <b>N</b> - 120.00 ± 0.0 °C - <b>N<sub>TB</sub></b> - 89 °C - <b>SmA<sub>b</sub></b>      (<b>Cr</b> - 121 °C - <b>N<sub>TB</sub></b>)</p>

### 3.1.1. CB7CB

The liquid crystal dimer CB7CB, the systematic name of which is 1",7"-bis(4-cyanobiphenyl-4'-yl)heptane, is the most famous **N<sub>TB</sub>**-forming compound. Indeed, the **N<sub>TB</sub>** phase was discovered with this material [7]. It was also the first compound (or at least one of the first) for which the structural and physical properties of the **N<sub>TB</sub>** phase were characterized, e.g., pitch [9,13,14], conical tilt angle [9,10,14], and dielectric constant [7]. CB7CB was also the compound used in the first detailed ECE study [9] (note that we repeat here the ECE experiment with CB7CB over a larger temperature range and with a significantly improved time resolution).

CB7CB was prepared following methods described previously in detail [7,20,38]. The transition temperatures obtained by DSC, are  $T(\text{N}_{\text{TB}}\text{-N}) = 376 \text{ K}$  and  $T(\text{N-I}) = 389 \text{ K}$ , respectively. These phase transitions were found to be first order [46]; the entropies of transition,  $\Delta S/R$ , are 0.34 and 0.31, respectively [38].

CB7CB has a positive dielectric anisotropy,  $\Delta\epsilon \sim +2$  in the **N<sub>TB</sub>** phase close to the transition [7]. As for the other materials presenting  $\Delta\epsilon > 0$ , in the ECE experiments we limit the duration of the applied high-field electric pulses to  $< 100 \mu\text{s}$  in order to avoid textural changes under the strong dielectric torque.

### 3.1.2. CB9CB

The dimer 1,9-bis(4-cyanobiphenyl-4'-yl) nonane (CB9CB) differs from CB7CB only by the length of the spacer linking the two cyanobiphenyl mesogenic units. The synthesis and characterisation of CB9CB have been described in detail elsewhere [15]. In contrast with CB7CB, CB9CB shows an enantiotropic **N<sub>TB</sub>** phase over a large ( $> 20 \text{ °C}$ ) temperature range. However, due to the similar chemical structures of these homologues, their physical properties are also similar, and in particular  $\Delta\epsilon \sim 2$  in the vicinity of the **N-N<sub>TB</sub>** transition. The entropies of the **I-N** and **N-N<sub>TB</sub>** transitions,  $\Delta S/R$ , are 0.33 and 0.08, respectively [15], indicating that the **N-N<sub>TB</sub>** transition is much more weakly first-order in character than seen for CB7CB.

### 3.1.3. CB6OCB

1-(4-cyanobiphenyl-4'-yloxy)-6-(4-cyanobiphenyl-4'-yl)hexane (CB6OCB) contains also two cyanobiphenyl mesogenic units, but linked by an alkoxy  $(\text{CH}_2)_6\text{O}$  spacer. The synthesis and characterisation of this dimer have been described in detail elsewhere

[15,16]. Due to the ether link on one side of the spacer, which results in a smaller bend-angle of the molecule, both nematic phases of CB6OCB, N and N<sub>TB</sub>, are enantiotropic and show significantly wider temperature ranges than for CB7CB. The entropy of the N-N<sub>TB</sub> transition is extremely small,  $\Delta S/R = 0.01$  [15], which indicates that the transition is much more weakly first-order in character than seen for CB7CB. Due to the similar chemical structures of these dimers, their physical properties are similar, in particular  $\Delta\epsilon \sim 2$  in the vicinity of the N-N<sub>TB</sub> transition.

### 3.1.4. BNA76

The bent-shaped dimer 1,7-bis[6-(4-hexyloxybenzoyloxy) naphthalene-2-yl]heptane (BNA76) was prepared following a synthetic route described earlier [39]. The molecular structure of BNA76 is quite different from those of the other three compounds studied here. Instead of cyanobiphenyls, the mesogenic units of BNA76 are benzoyloxy-naphthyl esters with relatively long alkyl terminal-chains. The phase sequence of BNA76 is richer than that of the cyanobiphenyl-based dimers as it presents three mesomorphic states – nematic, twist-bend nematic, and intercalated biaxial smectic A (SmA<sub>b</sub>). The entropy of the N-N<sub>TB</sub> transition is small [39],  $\Delta S/R = 0.05$ , which indicates a weak first-order transition, as expected [16,46] because of the wide temperature range of the N-phase. Due to the absence of large longitudinal dipoles in the mesogenic units, BNA76 shows a negative dielectric anisotropy,  $\Delta\epsilon < 0$ , and therefore no textural changes are observed in the N and N<sub>TB</sub> phases in our planar cells, even under strong fields ( $E \sim 20$  V/ $\mu\text{m}$ ). This allows us to apply in our ECE experiments arbitrarily long d.c. voltage pulses (or a.c. voltage bursts) without textural change issues. (Note that the cell behaviour is different in the SmA<sub>b</sub> phase : because of the phase biaxiality, textural transitions [8] are observed under voltages of  $\sim 4$  V. However, the SmA<sub>b</sub> phase is achiral and, therefore, as expected, it does not show any electroclinic response.)

### 3.2. Measurement technique

For the ECE measurements, the compounds were filled into optical cells with a small gap,  $d = 1.5$   $\mu\text{m}$ , (kindly provided by Nemoptic, France) by capillarity action. This cell thickness was required to obtain an optical retardation,  $\Delta L = d \cdot \Delta n$ , of the transmitted polarized light of wavelength  $\lambda$ , in the optimal range for the ECE measurements ( $\lambda/4 < \Delta L < 3\lambda/4$ ). Rubbed polyimide layers deposited on the cell surfaces provided a uniform planar alignment with a small pretilt (1-2°) in the nematic phase. The field was applied to the cell by transparent ITO electrodes with a small resistivity (4 Ohms per square).

In the nematic phase, all of the dimers showed good planar alignment allowing, if necessary, for the measurement of their physical and optical properties. On slow cooling through the N-N<sub>TB</sub> phase transition, we observed the growth of uniform monochiral N<sub>TB</sub> domains separated by domain walls. The typical size of these domains varied from tens to hundreds of micrometers, depending on the compound and cooling rate. On further N<sub>TB</sub>-N-N<sub>TB</sub> cycling, the domain pattern changed randomly without visible memory of the domain handedness.

After a few N<sub>TB</sub>-N-N<sub>TB</sub> cycles, the domains were sufficiently large to allow for ECE measurements in monochiral regions of at least  $50 \times 50$   $\mu\text{m}^2$  in size. Usually, a few tenths of a degree below the transition, the domains were reasonably uniform but, upon further cooling in most cases, the well-known stripe- and (at lower temperature) rope-instabilities [7] were observed. To avoid these instabilities, which can disturb the electro-optical response to the field, the temperature of the N<sub>TB</sub> phase was slowly decreased while superposing weak temperature oscillations (with typical amplitude  $\sim 1$  °C and frequency  $\sim 0.01$  Hz). During this process, an a.c. voltage ( $f = 10$  kHz,  $U < 6$  V) was switched on- and off- at about 0.1 Hz. This treatment progressively weakened the instabilities and was repeated until they no longer significantly disturbed the ECE measure-

ments or until they completely vanished (in the best case). The best results of this treatment were obtained for CB7CB that showed a uniform texture of the monodomains over a temperature range of more than 50 °C below the N-N<sub>TB</sub> transition, and the worst for CB6OCB, with only a 20 °C range.

A simple technique, previously described in more detail, was applied to measure the ECE response [9]. In the absence of the field, the N<sub>TB</sub> optical axis, **N**<sub>0</sub>, is parallel to the polarizer P (Fig. 4). When the field **E** is applied, the optical axis rotates in the plane of the cell by a small angle  $\alpha$  to a new orientation, **N**. With the analyzer, A, set at 45° with respect to P, the transmitted light intensity, *I*, is approximately a linear function of  $\alpha$  [9]:

$$I \cong \frac{1}{2} I_0 \left[ 1 - 4 \alpha \sin^2 \left( \frac{\pi \Delta L}{\lambda} \right) \right], \quad (7)$$

where *I*<sub>0</sub> is the intensity of the incident light. The sensitivity of the measurement is optimal for  $\Delta L \approx (m + 1/2) \lambda$  with *m* an integer. For our cell gap, *d* = 1.5 μm,  $\Delta L$  varies with temperature in the 150–250 nm range, resulting in a reasonably large slope for *I*( $\alpha$ ). To calibrate the measurements of  $\alpha$  without additional birefringence measurements, we measure directly, at each temperature, the slope of *I*( $\alpha$ ) by rotating the cell to a known fixed angle  $\alpha_0 = \pm 4^\circ$  (at fixed *I*<sub>0</sub> and *U* = 0).

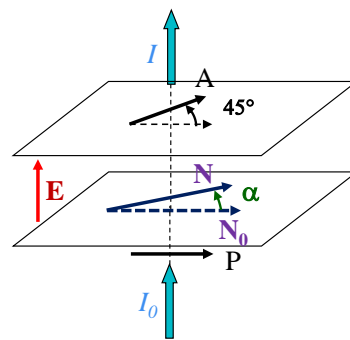


**Figure 4.** The optical geometry used for the ECE<sub>NTB</sub> measurements.

The cell is placed on the stage of a polarizing microscope (Leitz Ortholux) equipped with a light source with a stabilized d.c. voltage supply. The temperature of the sample is controlled with a precision of 0.01 °C using a Mettler HS82 hot-stage and a home-built PID temperature controller. The transmitted intensity is measured using a microphotometer (Leitz) mounted on the microscope and equipped with a photomultiplier tube (PMT). The measurement is local and limited to a small selected rectangular area (typically 40×40 μm<sup>2</sup>) in the image plane. To minimize the response time of the detection system, the current signal from the PMT is sent directly to a small resistive load, *R*<sub>L</sub> = 1 kΩ. The voltage drop on the charge is sent to a digital oscilloscope (DSO-X 2004A, Agilent), where it is accumulated for up to 64000 times to improve the signal-to-noise ratio. The typical error in  $\alpha$  is estimated to be less than 0.01° and the response time,  $\tau_{exp}$ , of the experimental setup, measured with a LED light source driven by short rectangular pulses, is about 160 ns. The main effect of the instrumental response time on the measured signal is an additional delay ( $\sim \tau_{exp}$ ) of the ECE response without a change in the slope of the ECE curve. Using a suitable fitting procedure taking into account this effect the error in the measured ECE response times can be reduced to only around 30 ns.

During the experiments, short voltage pulses (typically 10–40 μs) were applied to the ITO electrodes, resulting in a d.c. electric field directed along the cell normal which is also

the observation direction. The pulses were generated by an arbitrary wavefunction generator (TGA1241, TTI) and amplified by a fast high-voltage amplifier (Krohn-Hite 7602M) up to amplitudes in the range 15 – 120 V. The short duration of the pulses was required in the case of  $\Delta\epsilon > 0$  materials to avoid the reorientation of the  $N_{TB}$  helix under the strong dielectric torque. For BNA76, however,  $\Delta\epsilon < 0$ , and the dielectric torque stabilizes the planar alignment of the helix in our cells, and arbitrarily long pulses can be applied without destroying the uniform  $N_{TB}$  texture.

#### 4. Results

For all four compounds, the experimental results are in good qualitative agreement with the theoretically expected behaviour. Subject to square pulses, the ECE response is well fitted by an exponential law, with approximately the same on- and off- response times (Fig. 5 to improve). Moreover, as expected, the sign of the response is reversed when the measurement window is displaced from one monochiral domain to the next, which has the opposite handedness. This feature, as noted before [9,10], is direct evidence of the doubly-degenerate chiral structure of the  $N_{TB}$  phase.

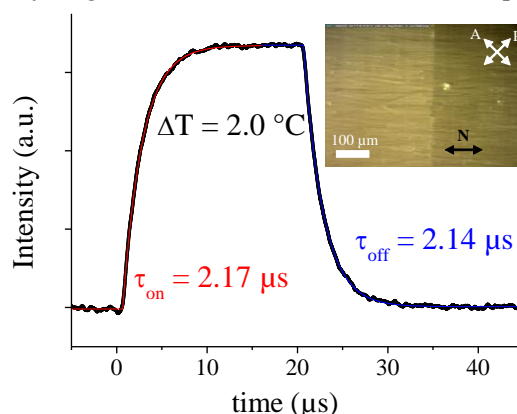


**Figure 5.** ECE<sub>NTB</sub> response (black open symbols) to a square d.c. pulse (15 V/μm, 20 μs) measured in a BNA76 monochiral domain. The solid lines are the best fits of the data with an exponential law for the rise (red) and the fall (blue) of the response. The inset shows two large monochiral uniform domains of opposite chirality observed with slightly uncrossed polarizers.

As expected from Eq. (5), the variation of  $\alpha$  with the field is linear. This is best demonstrated by applying bipolar triangular pulses, as shown in Fig. 6. The ECE response is proportional to the field, with only a small delay and distortion at the peaks of the signal (due to the finite response time of the ECE<sub>NTB</sub> effect). The change of the response sign with the sign of the field is also direct evidence that the macroscopic structure of the phase is chiral.

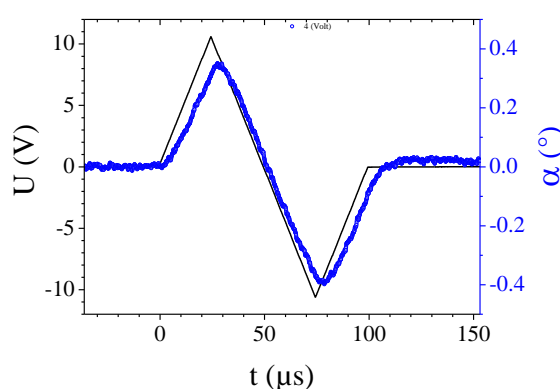


**Figure 6.** : CB6OCB at  $T = 108.05$  °C: time-evolution of the electroclinic tilt angle  $\alpha$  (blue open symbols, right axis) subject to a triangular voltage pulse (black line, left axis).

To compare the temperature dependences of the ECE response of the four compounds, we present later the results for each one in terms of  $c_\alpha(T)$  and  $\tau(T)$ . In addition, for each of them, we also present the best fit with a power law,  $c_\alpha(T) = cte \cdot (T_\alpha * -T)^{-\beta_\alpha}$  and  $\tau(T) = cte \cdot (T_\tau * -T)^{-\beta_\tau}$ , respectively. Note that, for the theoretical models, the critical temperature  $T^*$  should be the same for  $\alpha$  and  $\tau$ . This is, however, not confirmed experimentally. The best fit parameters for all the compounds under study are presented in Table 2.

#### 4.1. CB7CB

CB7CB, using which the  $N_{TB}$  phase was first confirmed experimentally [7], remains to date the most studied  $N_{TB}$  compound. In particular, it was the dimer for which the first detailed ECE experiment was reported [9]. However, this study presents a more recent experiment with better time resolution, wider temperature range, and a larger number of temperature data points. Although the present data are in excellent agreement with the previous, they provide better precision on the values of the fit parameters. The experimental results for  $c_\alpha(T)$  and  $\tau(T)$  over the whole temperature range of the  $N_{TB}$  phase are shown in Fig. 7.  $c_\alpha(T)$  is already small at the transition and it decreases further throughout the  $N_{TB}$  phase. At low temperature, it approaches a limiting value. Magnifying the  $c_\alpha(T)$  curve in the vicinity of the N- $N_{TB}$  phase transition (see inset) reveals a relatively large temperature range (99.5–100.2 °C) of biphasic coexistence, in good agreement with previous reports [7,9,10]. In the following discussion, we define the median temperature of this biphasic range,  $T_c = 99.85$  °C, as the experimentally observed N- $N_{TB}$  transition temperature (the same approach is used for the other compounds). The ECE response time is very short at the transition,  $\tau \approx 0.7$   $\mu$ s. Upon cooling, it decreases even further over a few °C, and then levels off at a value of about 0.23  $\mu$ s over the next 20 °C. Upon further cooling,  $\tau(T)$  grows exponentially, due to the Arrhenius temperature dependence of the rotational viscosity to which it is proportional (see Eq. (6) and the discussion section).

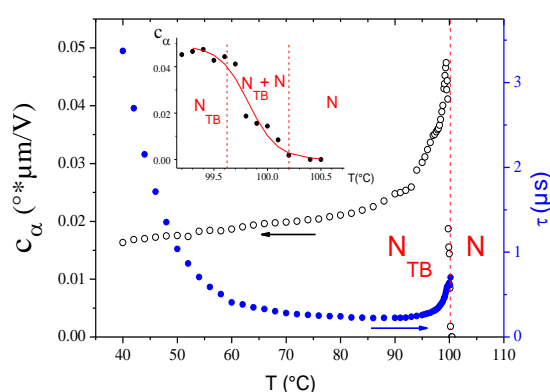


**Figure 7.** Temperature dependence of the ECE parameters,  $c_\alpha(T)$  and  $\tau(T)$ , measured in the  $N_{TB}$  phase of the dimer CB7CB. The inset shows a magnification of  $c_\alpha(T)$  in the relatively large N- $N_{TB}$  biphasic coexistence range.

As expected theoretically,  $c_\alpha(T)$  and  $\tau(T)$  follow power law dependences over a range of several °C below the N-N<sub>TB</sub> transition (Fig. 8), where the slow temperature variation of all the nematic parameters, except  $K_{33}$ , can be neglected. Moreover,  $c_\alpha(T)$  follows a power law dependence over the entire available temperature range whereas  $\tau(T)$  deviates from this, but only far from the transition. However, the critical temperatures  $T^*$  derived from these two fits are not the same and, in disagreement with the theoretical models, they differ from the experimental value of  $T_c$  by small but significant values,  $\Delta T_\alpha = T_\alpha^* - T_c = 0.20$  °C and  $\Delta T_\tau = T_\tau^* - T_c = 0.35$  °C.

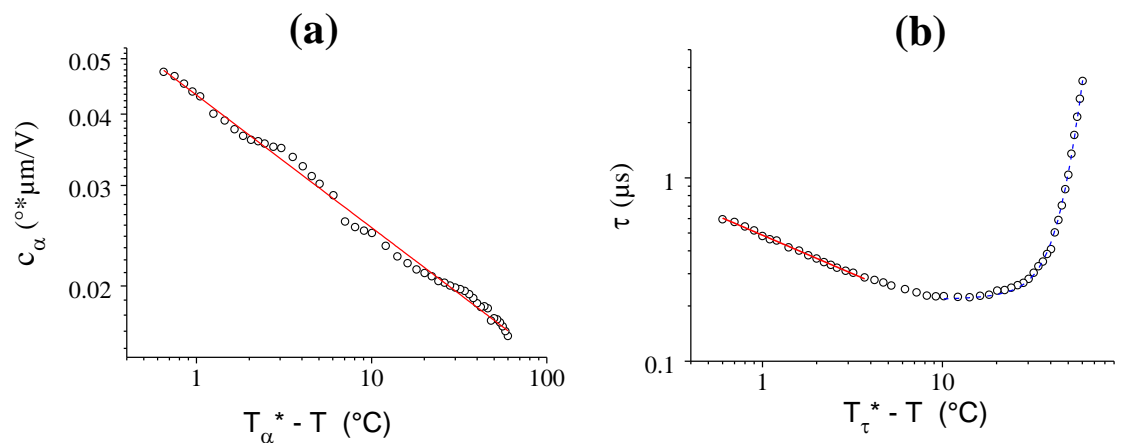


**Figure 8.** Best fits (red solid lines) of  $c_\alpha(T)$  and  $\tau(T)$  with power laws for CB7CB: (a) For  $c_\alpha(T)$ , the fit  $c_\alpha(T) = cte \cdot (T_\alpha^* - T)^{-\beta_\alpha}$  is good over the entire (60 °C) range under study, with  $T_\alpha^* = 100.05$  °C and  $\beta_\alpha = 0.23$ ; (b) For the response time, the law  $\tau(T) = cte \cdot (T_\tau^* - T)^{-\beta_\tau}$ , with  $T_\tau^* = 100.20$  °C and  $\beta_\tau = 0.42$ , fits the curve well only in a range of about 6 °C. At low temperature, the curve is well fitted by an exponential growth law (blue dashed curve).

#### 4.2. CB9CB

The dimer CB9CB is a homologue of CB7CB and differs from it only by the spacer length. The experimental results for  $c_\alpha(T)$  and  $\tau(T)$  are very similar to those of CB7CB (Fig. 9). Indeed,  $c_\alpha(T)$  is small at the transition, it decreases throughout the N<sub>TB</sub> phase and approaches a limiting value at low temperature. The N-N<sub>TB</sub> phase transition is very sharp, almost without any biphasic coexistence, and takes place at  $T_c = 107.00$  °C. At the transition, the ECE response time,  $\tau \approx 2.2$  µs, is slower than in CB7CB but it remains of the same order of magnitude. Upon cooling, it decreases further over a few °C, then levels off at about 0.36 µs and grows exponentially upon further cooling. However, even at  $T = 50$  °C, the response time remains rather fast,  $\tau \approx 1.1$  µs.



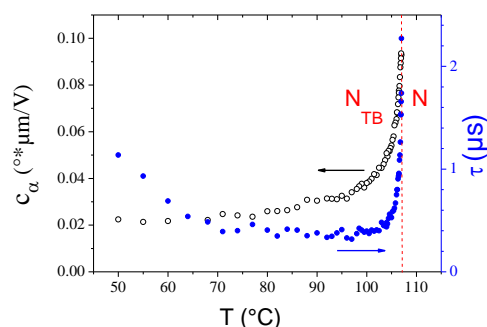


**Figure 9.** Temperature dependence of the ECE parameters,  $c_{\alpha}(T)$  and  $\tau(T)$ , measured in the  $N_{TB}$  phase of the bent-shaped dimer CB9CB. For this compound, the N- $N_{TB}$  biphasic coexistence temperature range is very narrow, almost undetectable.

As expected,  $c_{\alpha}(T)$  and  $\tau(T)$  follow power law dependences in the vicinity of the N- $N_{TB}$  transition (Fig. 10). As for CB7CB, the  $c_{\alpha}(T)$  curve is fitted well by the power law over the entire available temperature range whereas  $\tau(T)$  deviates from this far from the transition. The critical temperatures  $T^*$ , derived from the two fits, are again different and also differ from the experimental value of  $T_c$ , with  $\Delta T_{\alpha} = T_{\alpha}^* - T_c = 0.45$  °C and  $\Delta T_{\tau} = T_{\tau}^* - T_c = 0.14$  °C.

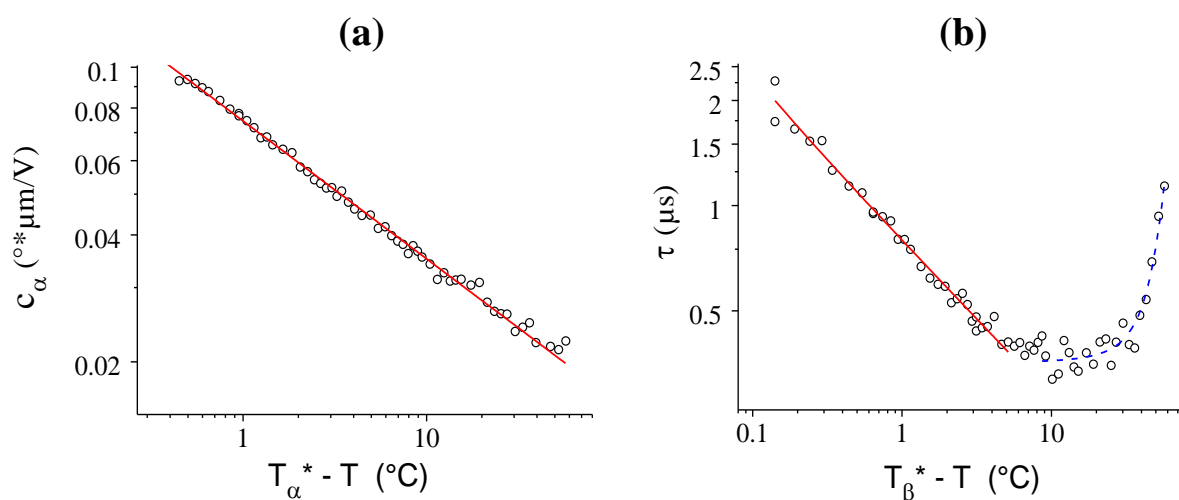


**Figure 10.** Best fits (red solid lines) of  $c_{\alpha}(T)$  and  $\tau(T)$  with power laws for CB9CB: (a) For  $c_{\alpha}(T)$ , the fit  $c_{\alpha}(T) = cte \cdot (T_{\alpha}^* - T)^{-\beta_{\alpha}}$  is good over the entire ( $> 60$  °C) range under study, with  $T_{\alpha}^* = 107.45$  °C and  $\beta_{\alpha} = 0.33$ ; (b) The power law  $\tau(T) = cte \cdot (T_{\tau}^* - T)^{-\beta_{\tau}}$ , with  $T_{\tau}^* = 100.14$  °C and  $\beta_{\tau} = 0.45$ , fits the curve well only in a range of about 5 °C. As for CB7CB, at low temperature, the curve is well fitted by an exponential growth law (blue dashed curve).

#### 4.3. CB6OCB

The dimer CB6OCB has approximately the same length as CB7CB but the spacer has a different chemical structure. Consequently, these two compounds differ in some of the physical properties of their nematic phases. For example, the nematic temperature range

of CB6OCB (48°C) is significantly larger than that of CB7CB (15 °C) and the N-N<sub>TB</sub> phase transition is almost second-order whereas that of CB7CB is weakly first-order. The experimental results for  $c_\alpha(T)$  and  $\tau(T)$  in the whole temperature range of the N<sub>TB</sub> phase are shown in Fig. 11. Note that, for this compound, the texture instabilities could not be completely suppressed below 95 °C, which reduced the quality of the data.  $c_\alpha(T)$  is small at the transition, it decreases throughout the N<sub>TB</sub> phase, and approaches a limiting value at low temperature. The N-N<sub>TB</sub> phase transition is sharp and takes place at  $T_c = 108.08$  °C, with a small biphasic coexistence range (108.05 – 108.10 °C). At the transition, the ECE response time,  $\tau \approx 7$  μs, is about one order of magnitude slower than in CB7CB. Upon cooling, it sharply decreases over a few °C and levels off to about 0.8 μs.

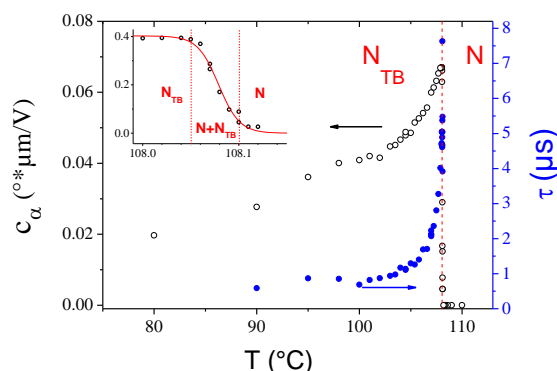


**Figure 11.** Temperature dependences of the ECE parameters,  $c_\alpha(T)$  and  $\tau(T)$ , measured in the N<sub>TB</sub> phase of the bent-shaped dimer CB6OCB. The inset shows a magnification of the N-N<sub>TB</sub> biphasic coexistence range.

In the vicinity of the N-N<sub>TB</sub> transition,  $c_\alpha(T)$  and  $\tau(T)$  follow power laws, like the previous compounds (Fig. 12). Both curves are fitted well by power laws over 10 °C below the phase transition. The critical temperatures  $T^*$  determined from the two fits are quite different and also differ from the experimental value of  $T_c$ , with  $\Delta T_\alpha = T_\alpha^* - T_c = 1.70$  °C and  $\Delta T_\tau = T_\tau^* - T_c = 0.36$  °C.

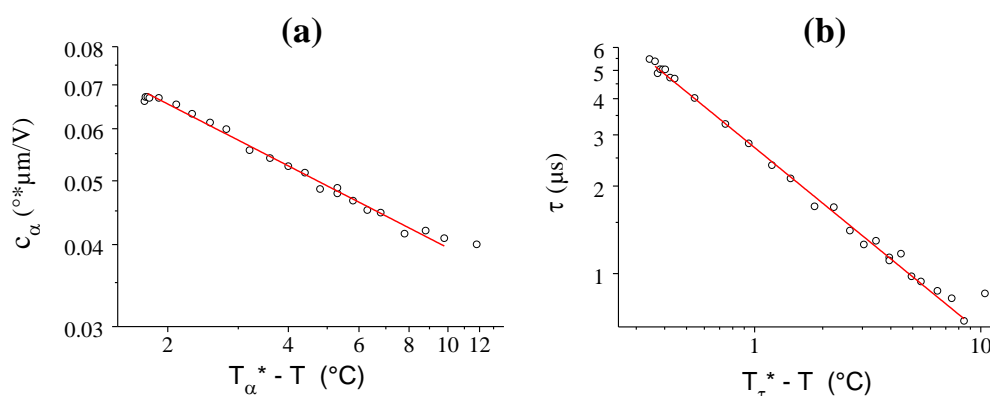


**Figure 12.** Best fits (solid red lines) of  $c_\alpha(T)$  and  $\tau(T)$  with power laws for CB6OCB: (a) For  $c_\alpha(T)$ , the fit  $c_\alpha(T) = cte \cdot (T_\alpha^* - T)^{-\beta_\alpha}$  provides  $T_\alpha^* = 109.78$  °C and  $\beta_\alpha = 0.31$ ; (b) The power law for the response time,  $\tau(T) = cte \cdot (T_\tau^* - T)^{-\beta_\tau}$ , gives  $T_\tau^* = 108.44$  °C and  $\beta_\tau = 0.64$ .

#### 4.4. BNA76

Like CB9CB, BNA76 presents a very sharp N-N<sub>TB</sub> phase transition that takes place at  $T_c = 120.00$  °C. As for the other compounds,  $c_\alpha(T)$  is small at the transition and decreases throughout the N<sub>TB</sub> phase (Fig. 13). The ECE response time is similar to that of CB9CB; it decreases from  $\tau \approx 7.2$   $\mu$ s at the transition to  $\tau \approx 1.0$   $\mu$ s at 95 °C.

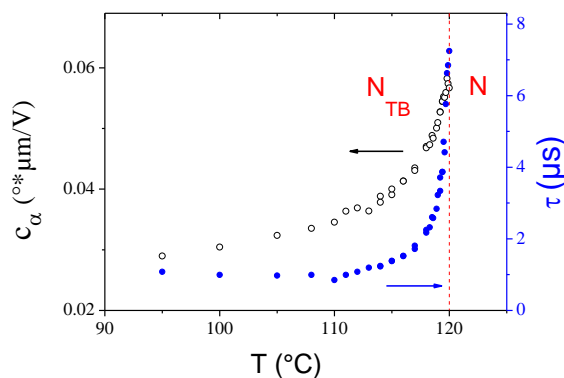


**Figure 13.** Temperature dependences of the ECE parameters,  $c_\alpha(T)$  and  $\tau(T)$ , measured in the N<sub>TB</sub> phase of the dimer BNA76. The N-N<sub>TB</sub> phase transition takes place at  $T_c = 120.00$  °C and the N-N<sub>TB</sub> biphasic coexistence temperature range is very narrow, almost undetectable.

Like the other cases, the  $c_\alpha(T)$  curve is fitted well by a power law over the entire available temperature range (Fig. 14), while  $\tau(T)$  follows a power law only close to the transition. The critical temperatures  $T^*$  derived from the two fits are again different and differ from the experimental value  $T_c$ , with  $\Delta T_\alpha = T_\alpha^* - T_c = 1.17$  °C and  $\Delta T_\tau = T_\tau^* - T_c = 0.50$  °C.

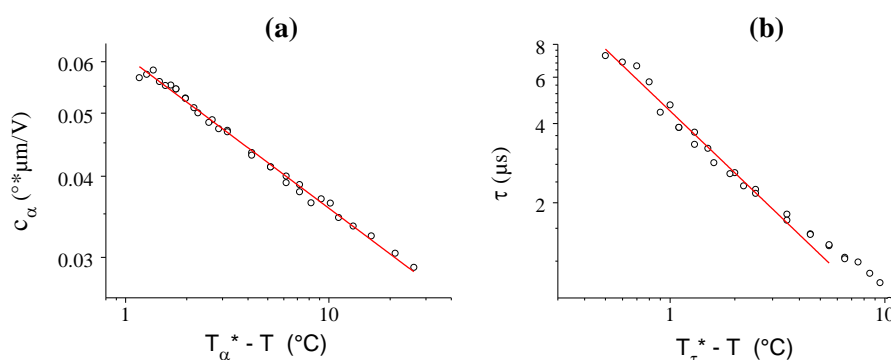


**Figure 14.** Best fits (solid red lines) of  $c_\alpha(T)$  and  $\tau(T)$  with power laws for BNA76: (a) For  $c_\alpha(T)$ , the fit  $c_\alpha(T) = cte \cdot (T_\alpha^* - T)^{-\beta_\alpha}$  is very good over the entire 25 °C range under study, with  $T_\alpha^* = 121.17$  °C and  $\beta_\alpha = 0.23$ ; (b) The power law  $\tau(T) = cte \cdot (T_\tau^* - T)^{-\beta_\tau}$ , with  $T_\tau^* = 120.50$  °C and  $\beta_\tau = 0.78$ , fits the curve well only in a range of about 6 °C.

**Table 2.** Comparison of the ECE<sub>N<sub>TB</sub></sub> parameters obtained from the power-law fits of the experimental results with the predictions of the theoretical models.

Compound	ECE experiment				Theory [9,31]			Theory [40]				
	$\Delta T_\alpha$	$\Delta T_\tau$	$\beta_\alpha$	$\beta_\tau$	$\Delta T$	$\beta_\alpha$	$\beta_\tau$	$\Delta T$	$T > T^* - \delta T$		$T < T^* - \delta T$	
	(°C)	(°C)			(°C)			(°C)	$\beta_\alpha$	$\beta_\tau$	$\beta_\alpha$	$\beta_\tau$
CB7CB	0.20	0.35	0.23	0.42	0	0.5	2.0	0	0.5	2.0	0.25	1.0
CB9CB	0.45	0.14	0.33	0.45	0	0.5	2.0	0	0.5	2.0	0.25	1.0
CB6OCB	1.70	0.36	0.31	0.64	0	0.5	2.0	0	0.5	2.0	0.25	1.0
BNA76	1.17	0.50	0.23	0.78	0	0.5	2.0	0	0.5	2.0	0.25	1.0

## 5. Discussion

The main  $\text{ECE}_{\text{NTB}}$  features that are expected theoretically are based on the macroscopic symmetry of the  $\text{N}_{\text{TB}}$  phase and its analogy with the chiral smectic A phase. Indeed, the geometry of the effect, with a torque, applied to the optic axis  $\mathbf{N}$  and proportional to the pseudo-vector  $\mathbf{h} \times \mathbf{E}$ , is only possible in a chiral system. Therefore, the mere existence of the electroclinic effect is a direct proof of the chiral structure of the  $\text{N}_{\text{TB}}$  phase and its layered or pseudo-layered organization. Similarly, the alternation of the sign of the  $\text{ECE}_{\text{NTB}}$  response from one monochiral domain to the next is direct evidence of the doubly-degenerate chirality of the phase. Moreover, the fact that the response is linear in the field reveals that the effect is not dielectric but flexo- or ferro-electric.

All of these expected features have already been observed in the first  $\text{ECE}_{\text{NTB}}$  experiments using CB7CB [9], giving an early confirmation of the heliconical (and helielectric) structure of the  $\text{N}_{\text{TB}}$  phase. Here, we show that this behaviour is typical for twist-bend nematics as it is observed for all of the four compounds under study. Indeed, for all compounds, close to the  $\text{N}$ - $\text{N}_{\text{TB}}$  transition temperature, we find that the amplitude of the electroclinic tilt of  $\mathbf{N}$  is small, of the order of  $0.5$ - $1^\circ$  for  $10 \text{ V}/\mu\text{m}$  (or  $c_\alpha < 0.1^\circ \text{V}/\mu\text{m}$ ). On cooling,  $c_\alpha$  decreases further, by a factor of 2 to 5, depending on the compound. The CG theory of the  $\text{N}_{\text{TB}}$  phase relates the value of  $c_\alpha$  close to the transition with the material constants in the nematic phase and the pitch  $p$  of the  $\text{N}_{\text{TB}}$  phase (see Eq. (5)). With the typical values of the constants available for the nematics, it has been deduced previously [9,25] from the small value of  $c_\alpha$  for CB7CB that the pitch is about 7 nm. This surprisingly small value was later confirmed by direct measurements [13,14,19] and is now accepted to be typical for this quantity.

Our study confirms this conclusion for the other three dimers. Moreover, assuming that the nematic constants  $(e_1 - e_3)$  and  $(K_{11} + K_{22})$  vary slowly in the vicinity of  $T_c$ , we conclude that the temperature dependence of  $c_\alpha$  is largely due to the variation of the pitch, i.e. that the pitch decreases with decreasing temperature. This behaviour of  $p(T)$ , which is theoretically predicted [5,34], agrees qualitatively with the resonant X-ray scattering experiments on CB7CB [19], which report a moderate decrease of  $p(T)$  below  $T_c$ . Our results for the other compounds (see Figs. 9,11,13) suggest that the decrease of  $p(T)$  on cooling is a typical feature for the bent-shaped dimers that form a  $\text{N}_{\text{TB}}$  phase. However, the agreement between the decrease ( $\approx 50\%$ ) of  $p(T)$  in the  $10^\circ \text{C}$

range below  $T_c$  deduced from Fig. 7 and that reported in [19] ( $< 20\%$ ) is not quantitative. This disagreement may be due to the assumptions of the theoretical model, such as, for example, neglecting the temperature dependence of the nematic constants in the vicinity of  $T_c$ , and the approximation that the nematic order tensor is continuous at the N-N<sub>TB</sub> transition and remains uniaxial in the N<sub>TB</sub> phase [5,31] despite the biaxial local symmetry of the phase. The resonant X-ray scattering experiments provide a direct measurement of  $p(T)$ , but their temperature dependence shows some hysteresis, which is due to the polydomain structure of the samples and the defect pinning that hinders the relaxation of the pitch to its equilibrium value after a temperature variation. Our ECE<sub>N<sub>TB</sub></sub> measurements do not suffer from this problem as no hysteresis of  $c_\alpha(T)$  is observed with our thin and well-aligned monodomain samples. Moreover, the smooth variation of  $c_\alpha(T)$  observed on heating/cooling at a rate of  $1\text{ }^\circ\text{C/min}$  indicates that the pitch follows, adiabatically, the temperature variation.

The ECE<sub>N<sub>TB</sub></sub> response times of the four dimers show the same behaviour as that reported in the previous experiments using CB7CB. The on- and off- response times are the same, as expected from Eq. (6), and they are very fast close to the N-N<sub>TB</sub> phase transition for all the compounds ( $\tau < 10\text{ }\mu\text{s}$ ). However, this initial value was found to vary by one order of magnitude, from  $\sim 0.7\text{ }\mu\text{s}$  for CB7CB up to  $\sim 7\text{ }\mu\text{s}$  for BNA76. We attribute this variation to the different material constants in Eq. (6) for the different dimers, in particular to the rotational viscosity  $\gamma_1$ , which varies significantly between the different nematogenic compounds. Indeed,  $\gamma_1$  is relatively small for the nematic compound 5CB [47], which is very close to the monomer unit of CB7CB and CB9CB. This correlates well with the faster ECE response that we report for these compounds.

The temperature dependence of the response time is also similar for the different dimers. On cooling below  $T_c$ ,  $\tau$  decreases rapidly in the first  $5\text{--}10\text{ }^\circ\text{C}$ ; then, it saturates to a  $\sim 20\text{ }^\circ\text{C}$  wide plateau, for which the ECE response is the fastest ( $\tau < 1\text{ }\mu\text{s}$ ); finally, on further cooling,  $\tau(T)$  grows exponentially, clearly due to the usual Arrhenius-law increase of the rotational viscosity.

Qualitatively, assuming typical values of the nematic constants (see the detailed discussion for CB7CB in [9]), the initial values of  $c_\alpha$  and  $\tau$  are consistent with those predicted theoretically in Eqs. (5-6). Similarly, the temperature dependences  $c_\alpha(T)$  and  $\tau(T)$  agree qualitatively with Eqs. (5-6): with the nematic constants assumed to vary only weakly, the initial fast decrease of the curves would largely be explained by the expected increase of the heliconical wavenumber and tilt angle; the plateau would be explained by the saturation of the N<sub>TB</sub> heliconical parameters; and the final increase of  $\tau(T)$ , which is absent for  $c_\alpha(T)$ , would be explained by the exponential growth of  $\gamma_1$  at low temperature. Moreover, as expected theoretically,  $c_\alpha(T)$  and  $\tau(T)$  follow a power law for at least  $5\text{ }^\circ\text{C}$  below the N-N<sub>TB</sub> transition. In fact, the power-law fit is excellent for  $c_\alpha(T)$  over a much larger temperature range, see for example, Figs. 8 and 10, which confirms that the nematic constants, apart from  $\gamma_1$ , vary only weakly with the temperature.

Despite this qualitative, or even semi-quantitative, agreement of our results with the CG theory, there are serious disagreements with the Landau models of the N-N<sub>TB</sub> phase transition. The main parameters derived from the power-law fits of  $c_\alpha(T)$  and  $\tau(T)$  are compared to the predictions of the theoretical models [31,40] in Table 2. Both models predict a second-order N-N<sub>TB</sub> transition and, therefore, that the critical temperature,  $T^*$ , of the power-laws should be identical to the measured transition temperature,  $T_c$  [31,40]. Theoretically, for a 2<sup>nd</sup>-order transition, there is no biphasic coexistence, but it is observed

experimentally for CB7CB and, although quite small,  $\sim 0.05$  °C, for CB6OCB, indicating that the transition for these compounds is in fact first-order. For the other two compounds, the biphasic coexistence is essentially zero, which shows that the transition is much closer to being second-order, as also indicated from the DSC data [15,38,39]. Nevertheless, for each compound, the critical temperature  $T^*$  obtained from the power-law fits of our data differs from the transition temperature  $T_c$ . This result disagrees with the two Landau-like theoretical models of the N-N<sub>TB</sub> transition considered here [31,40], and with the second-order transition predicted by other theoretical models, based on a Landau-like [48] or on a generalized Maier-Saupe [49] description of the N<sub>TB</sub> phase. Moreover, according to the models described in [31,40], the critical temperatures obtained from the fits of  $c_\alpha(T)$  and  $\tau(T)$  should be identical for each compound, which again disagrees with our measurements. Indeed, different critical temperatures were systematically obtained from the two fits,  $T_\alpha^* \neq T_\tau^* > T_c$ , which can be up to  $\sim 2$  °C higher than  $T_c$  (see Table 2). Quite surprisingly, at least for the case of  $T_\alpha^*$ , the difference with  $T_c$  is larger for the compounds CB6OCB and BNA76 that present a N-N<sub>TB</sub> transition almost second-order in nature and are therefore expected to be a better match to the theoretical prediction  $T_\alpha^* = T_\tau^* = T_c$ .

Another significant discrepancy with the predictions of the theoretical models is revealed by the critical exponents obtained from the power-law fits. Close to  $T^*$ , both models [31,40] predict  $\beta_\alpha = 0.5$  for the  $c_\alpha$ -exponent, which is largely governed by only the  $p(T)$  dependence. However, the experimental values are not universal and instead are spread around a value,  $\beta_\alpha \approx 0.25$ , that is half the predicted value. Therefore, the experimental results for  $\beta_\alpha$  are in reasonable agreement with the prediction of the model described in Ref. [40], but below the cross-over temperature,  $T^* - \delta T$ . Similarly,  $\beta_\tau$  varies significantly for the different dimers and instead are spread around the value  $\beta_\tau = 0.5$ , far lower than the theoretically expected value of 2 (Ref. [31] and Ref. [40] above  $T^* - \delta T$ ). Even the lower value,  $\beta_\tau = 1$ , predicted by the model of Ref. [40] below the cross-over temperature, is significantly higher than the experimental values. Here also, there is no clear correlation between the strength of the first-order N-N<sub>TB</sub> transition and the corresponding results for  $\beta_\tau$ .

To understand the origin of the discrepancy between experiments and theory, we need to consider in more detail the approximations used in the models. The main features of the ECE<sub>N<sub>TB</sub></sub> effect (linear response to the field, opposite signs of the electroclinic tilt in monochiral domains with opposite handedness, geometry of the effect with deviation of the optic axis under field  $\delta \mathbf{N} \propto \mathbf{E} \times \mathbf{N}$ ) are only based, in the CG approach, on the macroscopic symmetry of the N<sub>TB</sub> phase and its analogy with the symmetry of the SmA\* phase [31]. These main features are indeed observed for all the compounds studied, confirming once more the now well-established heliconical structure of the phase. Moreover, the small amplitude of the electroclinic tilt ( $\alpha < 1^\circ$ ) and its extremely fast response time ( $\tau < 10$   $\mu$ s) reveal qualitatively that the heliconical pitch is very small, of the order of 10 nm. (This conclusion follows directly from the analogy with the flexoelectric effect in the cholesteric phase [44] and the order of magnitude of the nematic constants involved.)

To reach a more quantitative description and to calculate the values of the ECE parameters and their temperature dependences,  $c_\alpha(T)$  and  $\tau(T)$ , the CG approach must rely on a microscopic theoretical model of the N-N<sub>TB</sub> transition. Any one of the two analytical Landau-like models considered here [31,40] leads to the simple expressions in Eqs. (5-6), which involve the nematic constants  $e_1 - e_3$ ,  $K_{11} + K_{22}$ , and  $\gamma_1$ . Unfortun-

nately, most of these constants have not been measured for any  $N_{TB}$ -forming compound, even in its nematic phase, and their behaviour in the  $N_{TB}$  phase and across the  $N$ - $N_{TB}$  transition remains unknown. Therefore, to compare our measurements with the theory, additional approximations must be made, namely that the nematic constants remain continuous at the transition and vary slowly with temperature in the  $N_{TB}$  phase (compared to the fast temperature dependence of the pitch and of the heliconical angle in the vicinity of the transition). However, this approximation, which is inspired by the prediction of the Landau-like models that the  $N$ - $N_{TB}$  transition is second-order, is questionable and its failure may explain to some extent the disagreement between the experimental results and the theoretical predictions.

The two analytical Landau-like models assume, explicitly [31] or implicitly [40], that the nematic order parameter  $S$  is continuous at the  $N$ - $N_{TB}$  transition. This assumption, leading to a second-order phase transition, denies the experimentally reported weakly first-order character of the transition [15,38,39], and the observed jump of the scalar order parameter  $S$  for CB7CB [10]. Further development of the models taking into account the coupling between  $S$  and the structural  $N_{TB}$  parameters,  $\theta_0$  and  $p$ , may lead to a first-order transition and therefore to finite values of  $\theta_0$  and  $p$  at the transition. This should also alter the power-laws expected for these parameters and, consequently, for  $c_\alpha(T)$  and  $\tau(T)$ , leading hopefully to better agreement with the experiments.

Actually, Lopez et al. [46] have already proposed a Landau-like model of the  $N$ - $N_{TB}$  phase transition that takes into account the jump of the nematic order parameter tensor,  $\mathbf{Q}$ , at the  $N$ - $N_{TB}$  transition and the coupling of  $\mathbf{Q}$  with the  $N_{TB}$  order parameter  $\sin \theta_0$ . This model predicts a first-order  $N$ - $N_{TB}$  transition, with strength decreasing with the thermal range of stability of the nematic phase above the  $N_{TB}$  phase. This prediction is in excellent agreement with the experimental observations for a large number of  $N_{TB}$ -forming compounds and with the calorimetric data for several mesogenic dimers and mixtures [46], including CB6OCB [16]. We expect that a future CG theory of the  $ECE_{NTB}$ , based on this improved Landau model, will provide a better agreement with our present experimental results.

Another possible improvement of the theoretical models might be to take explicitly into account the biaxiality of the nematic order parameter tensor,  $\mathbf{Q}$ , in the  $N_{TB}$  phase. Indeed, even in the  $N$  phase, the bend distortion breaks the revolution symmetry of the nematic phase and  $\mathbf{Q}$  becomes slightly biaxial. Due to the strong spontaneous bend of the  $N_{TB}$  phase, the resulting biaxiality of  $\mathbf{Q}$  (which is again the primary order parameter of the phase) might become important as it was recently reported to lead to important changes of the phase behaviour under an applied field [42]. Because the bend distortion, and therefore the biaxiality of the order tensor  $\mathbf{Q}$ , strongly depends on the temperature, taking this dependence into account could lead to significant changes in the theoretically predicted behaviour for  $c_\alpha(T)$  and  $\tau(T)$ , in better agreement with the experimental results.

## 6. Conclusions

We report here an extensive study of the electroclinic effect in the  $N_{TB}$  phase of four mesogenic dimers. The  $ECE_{NTB}$  response is observed over the whole  $N_{TB}$  temperature range of the compounds (more than 60 °C wide for CB9CB). The amplitude of the effect is very small at the phase transition ( $\alpha \sim 1^\circ$  for  $E = 10 \text{ V}/\mu\text{m}$ ) and decreases further on cooling. As reported previously for CB7CB [9], the on- and off-  $ECE$  response times are equal and very short, typically in the microsecond range. This feature is very attractive for fast applications but has not yet been exploited because of the small amplitude of the electroclinic tilt. Qualitatively, our results are similar for all four compounds, despite their different physical properties including, for example, different signs of the dielectric

anisotropy, and different strength of the weakly first-order phase transition. The amplitude and the response time are largely related to the value of the heliconical pitch. Therefore, any practical application of the  $ECE_{NTB}$  might only be expected if compounds with larger  $N_{TB}$  pitches ( $\sim 30 - 50$  nm) are discovered.

The measured temperature dependences of the ECE parameters,  $c_a(T)$  and  $\tau(T)$ , follow power laws in the vicinity of the phase transition, as expected. However, as summarized in Table 2, the best-fit parameters of this data differ substantially from the theoretically expected ones. We attribute this discrepancy to the assumptions made in the data interpretation process and in the theoretical models [31,40] themselves. In particular, we point out that better agreement might be expected from improved models taking into account two factors so far neglected: the coupling of the nematic order parameter with the parameters defining the  $N_{TB}$  heliconical structure and the biaxiality of the nematic order parameter tensor in the  $N_{TB}$  phase.

**Author Contributions:** Conceptualization, Claire Meyer and Ivan Dozov; Investigation, Patrick Davidson, Geoffrey Luckhurst, Irena Dokli, Anamarija Knežević, Andreja Lesac, Daniel Paterson, Rebecca Walker, John Storey and Corrie Imrie; Methodology, Claire Meyer, Geoffrey Luckhurst and Ivan Dozov; Writing – original draft, Ivan Dozov; Writing – review & editing, Patrick Davidson, Geoffrey Luckhurst, Andreja Lesac and Corrie Imrie. All authors have read and agreed to the published version of the manuscript.

**Funding:** This research was funded by the Croatian Science Foundation (Grant No. IP-2019-04-7978); by the Agence Nationale pour la Recherche ANR (France) through Grant BESTNEMATICS, No. ANR-15-CE24-0012; by the French-Croatian bilateral program COGITO; by the Université de Picardie Jules Verne, Amiens, France;

**Conflicts of Interest:** The authors declare no conflict of interest.



## References

1. Frank, F.C. On the theory of liquid crystals. *Disc. Farad. Soc.* **1958**, *25*, 19-28, doi:10.1039/df9582500019.
2. Freiser, M.J. Ordered states of a nematic liquid *Phys. Rev. Lett.* **1970**, *24*, 1041, doi:10.1103/PhysRevLett.24.1041.
3. Meyer, R.B. In *Molecular Fluids*, Balian, R., Weill, G., Eds.; Balian, R., Weill, G., Eds.; Les Houches Summer School in Theoretical Physics; Gordon and Breach: New York, 1976; Volume XXV-1973 of *Les Houches Summer School in Theoretical Physics*, pp. 273-373.
4. Lorman, V.L.; Mettout, B. Unconventional mesophases formed by condensed vector waves in a medium of achiral molecules. *Phys. Rev. Lett.* **1999**, *82*, 940-943, doi:10.1103/PhysRevLett.82.940.
5. Dozov, I. On the spontaneous symmetry breaking in the mesophases of achiral banana-shaped molecules. *Europhys. Lett.* **2001**, *56*, 247.
6. Memmer, R. Liquid crystal phases of achiral banana-shaped molecules: a computer simulation study. *Liq. Cryst.* **2002**, *29*, 483-496, doi:10.1080/02678290110104586.
7. Cestari, M.; Diez-Berart, S.; Dunmur, D.A.; Ferrarini, A.; de la Fuente, M.R.; Jackson, D.J.B.; Lopez, D.O.; Luckhurst, G.R.; Perez-Jubindo, M.A.; Richardson, R.M.; et al. Phase behavior and properties of the liquid-crystal dimer 1',7'-bis(4-cyanobiphenyl-4'-yl) heptane: A twist-bend nematic liquid crystal. *Phys. Rev. E* **2011**, *84*, 031704, doi:10.1103/PhysRevE.84.031704.
8. Meyer, C.; Davidson, P.; Constantin, D.; Sergan, V.; Stoenescu, D.; Knezevic, A.; Dokli, I.; Lesac, A.; Dozov, I. Freedericksz-Like Transition in a Biaxial Smectic-A Phase. *Phys. Rev. X* **2021**, *11*, 031012, doi:10.1103/PhysRevX.11.031012.
9. Meyer, C.; Luckhurst, G.R.; Dozov, I. Flexoelectrically Driven Electroclinic Effect in the Twist-Bend Nematic Phase of Achiral Molecules with Bent Shapes. *Phys. Rev. Lett.* **2013**, *111*, 067801, doi:10.1103/PhysRevLett.111.067801.
10. Meyer, C.; Luckhurst, G.R.; Dozov, I. The temperature dependence of the heliconical tilt angle in the twist-bend nematic phase of the odd dimer CB7CB. *J. Mater. Chem.* **2015**, *3*, 318-328, doi:10.1039/c4tc01927j.
11. Imrie, C.T.; Walker, R.; Storey, J.M.D.; Gorecka, E.; Pociecha, D. Liquid Crystal Dimers and Smectic Phases from the Intercalated to the Twist-Bend. *Crystals* **2022**, *12*, 1245, doi:10.3390/cryst12091245.
12. Mandle, R.J. A Ten-Year Perspective on Twist-Bend Nematic Materials. *Molecules* **2022**, *27*, 2689, doi:10.3390/molecules27092689.
13. Borshch, V.; Kim, Y.K.; Xiang, J.; Gao, M.; Jakli, A.; Panov, V.P.; Vij, J.K.; Imrie, C.T.; Tamba, M.G.; Mehl, G.H.; et al. Nematic twist-bend phase with nanoscale modulation of molecular orientation. *Nat. Commun.* **2013**, *4*, 2635 doi:10.1038/ncomms3635.
14. Chen, D.; Porada, J.H.; Hooper, J.B.; Klitnick, A.; Shen, Y.; Tuchband, M.R.; Korblova, E.; Bedrov, D.; Walba, D.M.; Glaser, M.A.; et al. Chiral heliconical ground state of nanoscale pitch in a nematic liquid crystal of achiral molecular dimers. *PNAS* **2013**, *110*, 15931-15936, doi:10.1073/pnas.1314654110.
15. Paterson, D.A.; Abberley, J.P.; Harrison, W.T.; Storey, J.M.; Imrie, C.T. Cyanobiphenyl-based liquid crystal dimers and the twist-bend nematic phase. *Liq. Cryst.* **2017**, *44*, 127-146, doi:10.1080/02678292.2016.1274293.
16. Paterson, D.A.; Gao, M.; Kim, Y.K.; Jamali, A.; Finley, K.L.; Robles-Hernandez, B.; Diez-Berart, S.; Salud, J.; de la Fuente, M.R.; Timimi, B.A.; et al. Understanding the twist-bend nematic phase: the characterisation of 1-(4-cyanobiphenyl-4'-yloxy)-6-(4-cyanobiphenyl-4'-yl)hexane (CB6OCB) and comparison with CB7CB.

- Soft Matter* **2016**, *12*, 6827–6840, doi:10.1039/c6sm00537c.
17. Robles-Hernandez, B.; Sebastian, N.; Rosario de la Fuente, M.; Lopez, D.O.; Diez-Berart, S.; Salud, J.; Ros, M.B.; Dunmur, D.A.; Luckhurst, G.R.; Timimi, B.A. Twist, tilt, and orientational order at the nematic to twist-bend nematic phase transition of 1',9'-bis(4-cyanobiphenyl-4'-yl) nonane: A dielectric,  $^2\text{H}$  NMR, and calorimetric study. *Phys. Rev. E* **2015**, *92*, 062505, doi:10.1103/PhysRevE.92.062505.
  18. Salamonczyk, M.; Vaupotic, N.; Pociecha, D.; Wang, C.; Zhu, C.; Gorecka, E. Structure of nanoscale-pitch helical phases: blue phase and twist-bend nematic phase resolved by resonant soft X-ray scattering. *Soft Matter* **2017**, *13*, 6694–6699, doi:10.1039/c7sm00967d.
  19. Zhu, C.; Tuchband, M.R.; Young, A.; Shuai, M.; Scarbrough, A.; Walba, D.M.; MacLennan, J.E.; Wang, C.; Hexemer, A.; Clark, N.A. Resonant Carbon K-Edge Soft X-Ray Scattering from Lattice-Free Heliconical Molecular Ordering: Soft Dilative Elasticity of the Twist-Bend Liquid Crystal Phase. *Phys. Rev. Lett.* **2016**, *116*, 147803.
  20. Jokisaari, J.P.; Luckhurst, G.R.; Timimi, B.A.; Zhu, J.F.; Zimmermann, H. Twist-bend nematic phase of the liquid crystal dimer CB7CB: orientational order and conical angle determined by Xe-129 and H-2 NMR spectroscopy. *Liq. Cryst.* **2015**, *42*, 708–721, doi:10.1080/02678292.2015.1037576.
  21. Adlem, K.; Copic, M.; Luckhurst, G.R.; Mertelj, A.; Parri, O.; Richardson, R.M.; Snow, B.D.; Timimi, B.A.; Tuffin, R.P.; Wilkes, D. Chemically induced twist-bend nematic liquid crystals, liquid crystal dimers, and negative elastic constants. *Phys. Rev. E* **2013**, *88*, 022503, doi:10.1103/PhysRevE.88.022503.
  22. Panov, V.P.; Vij, J.K.; Balachandran, R.; Borshch, V.; Lavrentovich, O.D.; Tamba, M.G.; Mehl, G.H. Properties of the self-deforming Ntb phase in mesogenic dimers. In *Liquid Crystals Xvii*, Khoo, I.C., Ed.; Proceedings of SPIE; 2013; Volume 8828.
  23. Dawood, A.A.; Grossel, M.C.; Luckhurst, G.R.; Richardson, R.M.; Timimi, B.A.; Wells, N.J.; Yousif, Y.Z. Twist-bend nematics, liquid crystal dimers, structure-property relations. *Liq. Cryst.* **2017**, *44*, 106–126, doi:10.1080/02678292.2017.1290576.
  24. Mandle, R.J.; Cowling, S.J.; Goodby, J.W. Combined Microscopy, Calorimetry and X-ray Scattering Study of Fluorinated Dimesogens. *Sci. Rep.* **2017**, *7*, doi:10.1038/s41598-017-12799-1.
  25. Meyer, C.; Luckhurst, G.R.; Dozov, I. Broken-symmetry nematic banana phases: Predictions and reality, presented at 24th International Liquid Crystal Conference, August 19th - 24th 2012, Mainz, Germany.
  26. Lewandowski, W.; Vaupotic, N.; Pociecha, D.; Gorecka, E.; Liz-Marzan, L.M. Chirality of Liquid Crystals Formed from Achiral Molecules Revealed by Resonant X-Ray Scattering. *Adv. Mater.* **2020**, *32*, 1905591, doi:10.1002/adma.201905591.
  27. Mandle, R.J.; Goodby, J.W. Order parameters, orientational distribution functions and heliconical tilt angles of oligomeric liquid crystals. *Phys. Chem. Chem. Phys.* **2019**, *21*, 6839–6843, doi:10.1039/c9cp00736a.
  28. Meyer, C.; Stoenescu, D.; Luckhurst, G.R.; Davidson, P.; Dozov, I. Smectic-like batonnets in nematic/twist-bend nematic biphasic samples. *Liq. Cryst.* **2017**, *44*, 232–243, doi:10.1080/02678292.2016.1218962.
  29. Salili, S.M.; Kim, C.; Sprunt, S.; Gleeson, J.T.; Parri, O.; Jákli, A. Flow properties of a twist-bend nematic liquid crystal. *RSC Adv.* **2014**, *4*, 57419–57423, doi:10.1039/c4ra10008e.
  30. Meyer, C. Nematic twist-bend phase under external constraints. *Liq. Cryst.* **2016**, *43*, 2144–2162, doi:10.1080/02678292.2016.1204635.
  31. Meyer, C.; Dozov, I. Local distortion energy and coarse-grained elasticity of the twist-bend nematic phase. *Soft*

- Matter* **2016**, *12*, 574–580, doi:10.1039/c5sm02018b.
32. Dozov, I.; Meyer, C. Analogy between the twist-bend nematic and the smectic A phases and coarse-grained description of the macroscopic N-TB properties. *Liq. Cryst.* **2017**, *44*, 4–23, doi:10.1080/02678292.2016.1226972.
  33. de Gennes, P.G. An analogy between superconductors and smectics A. *Solid State Commun.* **1972**, *10*, 753–756, doi:10.1016/0038-1098(72)90186-X
  34. Shamid, S.M.; Dhakal, S.; Selinger, J.V. Statistical mechanics of bend flexoelectricity and the twist-bend phase in bent-core liquid crystals. *Phys. Rev. E* **2013**, *87*, 052503, doi:10.1103/PhysRevE.87.052503.
  35. Garoff, S.; Meyer, R.B. Electro-clinic effect at AC phase-change in a chiral smectic liquid-crystal. *Phys. Rev. Lett.* **1977**, *38*, 848–851, doi:10.1103/PhysRevLett.38.848.
  36. Panov, V.P.; Balachandran, R.; Nagaraj, M.; Vij, J.K.; Tamba, M.G.; Kohlmeier, A.; Mehl, G.H. Microsecond linear optical response in the unusual nematic phase of achiral bimesogens. *Appl. Phys. Lett.* **2011**, *99*, 261903, doi:10.1063/1.3671996.
  37. Meyer, C.; Dozov, I.; Davidson, P.; Luckhurst, G.R.; Dokli, I.; Knezevic, A.; Lesac, A. Electric-field effects in the twist-bend nematic phase. In *Emerging Liquid Crystal Technologies Xiii*, Chien, L.C., Broer, D.J., Musevic, I., Chigrinov, V.G., Eds.; Proceedings of SPIE; 2018; Volume 10555.
  38. Barnes, P.J.; Douglass, A.G.; Heeks, S.K.; Luckhurst, G.R. An enhanced odd even effect of liquid-crystal dimers orientational order in the alpha, omega-bis(4'-cyanobiphenyl-4-yl)alkanes. *Liq. Cryst.* **1993**, *13*, 603–613, doi:10.1080/02678299308026332.
  39. Knežević, A.; Sapunar, M.; Buljan, A.; Dokli, I.; Hameršak, Z.; Kontrec, D.; Lesac, A. Fine-tuning the effect of  $\pi$ – $\pi$  interactions on the stability of the N<sub>TB</sub> phase. *Soft Matter* **2018**, *14*, 8466–8474, doi:10.1039/c8sm01569d.
  40. Parsouzi, Z.; Shamid, S.M.; Borshch, V.; Challa, P.K.; Baldwin, A.R.; Tamba, M.G.; Welch, C.; Mehl, G.H.; Gleeson, J.T.; Jakli, A.; et al. Fluctuation Modes of a Twist-Bend Nematic Liquid Crystal. *Phys. Rev. X* **2016**, *6*, 021041, doi:10.1103/PhysRevX.6.021041.
  41. Pajak, G.; Longa, L.; Chrzanowska, A. Nematic twist-bend phase in an external field. *PNAS* **2018**, *115*, E10303–E10312, doi:10.1073/pnas.1721786115.
  42. Meyer, C.; Blanc, C.; Luckhurst, G.R.; Davidson, P.; Dozov, I. Biaxiality-driven twist-bend to splay-bend nematic phase transition induced by an electric field. *Sci. Adv.* **2020**, *6*, eabb8212, doi:10.1126/sciadv.abb8212.
  43. Panov, V.P.; Song, J.K.; Mehl, G.H.; Vij, J.K. The Beauty of Twist-Bend Nematic Phase: Fast Switching Domains, First Order Freedericksz Transition and a Hierarchy of Structures. *Crystals* **2021**, *11*, 060621, doi:10.3390/cryst11060621.
  44. Patel, J.S.; Meyer, R.B. Flexoelectric electrooptics of a cholesteric liquid-crystal. *Phys. Rev. Lett.* **1987**, *58*, 1538–1540, doi:10.1103/PhysRevLett.58.1538.
  45. Meyer, R.B. Piezoelectric effects in liquid crystals *Phys. Rev. Lett.* **1969**, *22*, 918, doi:10.1103/PhysRevLett.22.918.
  46. López, D.O.; Robles-Hernandez, B.; Salud, J.; de la Fuente, M.R.; Sebastian, N.; Diez-Berart, S.; Jaen, X.; Dunmur, D.A.; Luckhurst, G.R. Miscibility studies of two twist-bend nematic liquid crystal dimers with different average molecular curvatures. A comparison between experimental data and predictions of a Landau mean-field theory for the N<sub>TB</sub>–N phase transition. *Phys. Chem. Chem. Phys.* **2016**, *18*, 4394–4404, doi:10.1039/c5cp07605f.
  47. Wu, S.-T.; Wu, C.-S. Experimental confirmation of the Osipov-Terentjev theory on the viscosity of nematic

liquid crystals. *Phys. Rev. A* **1990**, *42*, 2219-2227, doi:10.1103/PhysRevA.42.2219.

48. Kats, E.I.; Lebedev, V.V. Landau theory for helical nematic phases. *JETP Lett.* **2014**, *100*, 110-113, doi:10.1134/s0021364014140070.

49. Greco, C.; Luckhurst, G.R.; Ferrarini, A. Molecular geometry, twist-bend nematic phase and unconventional elasticity: a generalised Maier-Saupe theory. *Soft Matter* **2014**, *10*, 9318-9323, doi:10.1039/c4sm02173h.